

Sketching sparse low-rank matrices with near-optimal sample- and time-complexity using message passing

Xiaoqi Liu* and Ramji Venkataramanan

November 8, 2022

Abstract

We consider the problem of recovering an $n_1 \times n_2$ low-rank matrix with k -sparse singular vectors from a small number of linear measurements (sketch). We propose a sketching scheme and an algorithm that can recover the singular vectors with high probability, with a sample complexity and running time that both depend only on k and not on the ambient dimensions n_1 and n_2 . Our sketching operator, based on a scheme for compressed sensing by Li et al. [1] and Bakshi et al. [2], uses a combination of a sparse parity check matrix and a partial DFT matrix. Our main contribution is the design and analysis of a two-stage iterative algorithm which recovers the singular vectors by exploiting the simultaneously sparse and low-rank structure of the matrix. We derive a nonasymptotic bound on the probability of exact recovery, which holds for any $n_1 \times n_2$ sparse, low-rank matrix. We also show how the scheme can be adapted to tackle matrices that are approximately sparse and low-rank. The theoretical results are validated by numerical simulations and comparisons with existing schemes that use convex programming for recovery.

1 Introduction

We consider the problem of *sketching* a large data matrix which is low-rank with sparse singular vectors. A sketch is a compressed representation of the matrix, obtained via linear measurements of the matrix entries [3, 4]. The goal is to design a sketching scheme so that the singular vectors can be efficiently recovered from a sketch of a much smaller dimension.

Given a data matrix $\mathbf{X} \in \mathbb{R}^{n_1 \times n_2}$, its sketch $\mathbf{y} \in \mathbb{C}^m$ is obtained as $\mathbf{y} = \mathcal{A}(\mathbf{X})$, where \mathcal{A} is a linear operator defined via m prespecified matrices $\mathbf{A}_1, \dots, \mathbf{A}_m \in \mathbb{C}^{n_1 \times n_2}$. The entries of the sketch are:

$$y_i = \text{trace}(\mathbf{A}_i^T \mathbf{X}) = \sum_{j=1}^{n_1} \sum_{\ell=1}^{n_2} (A_i)_{j,\ell} X_{j,\ell}, \quad i = 1, \dots, m. \quad (1)$$

We consider data matrices \mathbf{X} of the form

$$\mathbf{X} = \mathbf{X}_0 + \mathbf{W}, \quad (2)$$

*Xiaoqi Liu was supported in part by a Schlumberger Cambridge International Scholarship funded by the Cambridge Trust. X. Liu and R. Venkataramanan are with the Department of Engineering, University of Cambridge. Email: {x1394, rv285}@cam.ac.uk. This paper was presented in part at the 2022 IEEE International Symposium on Information Theory.

with

$$\mathbf{X}_0 = \sum_{i=1}^r \lambda_i \mathbf{v}_i \mathbf{v}_i^T \text{ (symmetric case), or } \mathbf{X}_0 = \sum_{i=1}^r \sigma_i \mathbf{u}_i \mathbf{v}_i^T \text{ (non-symmetric case).} \quad (3)$$

In the symmetric case, $\lambda_1 \geq \lambda_2 \geq \dots \geq \lambda_r$ are the eigenvalues, $\{\mathbf{v}_i\}_{i \in [r]}$ are the corresponding unit-norm eigenvectors. In the non-symmetric case, $\sigma_1 \geq \sigma_2 \geq \dots \geq \sigma_r > 0$ are the singular values, and $\{\mathbf{u}_i, \mathbf{v}_i\}_{i \in [r]}$ the corresponding unit-norm singular vectors. In both cases, \mathbf{W} is a noise matrix (assumed to be symmetric when \mathbf{X}_0 is symmetric). Letting $n := \min(n_1, n_2)$, we consider the regime where n grows and the rank r of \mathbf{X}_0 is a constant that does not scale with n . In the rest of the paper, we refer to the $\{\mathbf{v}_i\}$ in the symmetric case and the $\{\mathbf{u}_i, \mathbf{v}_i\}$ in the non-symmetric case as *signal vectors*.

Sparsity constraint We assume that the signal vectors are k -sparse, i.e., they each have at most k nonzero entries, where $k \ll n$, and both k and n are large. This is a regime that is particularly relevant in applications such as genomics and neuroscience, where n is very large because of the vast number of features and samples, but the number of factors k determining the structure of the data may be much smaller [5, 6].

The goal is to design a sketching operator \mathcal{A} and an efficient algorithm to recover the signal vectors from the sketch \mathbf{y} . In particular, we want the sample complexity and the running time of the algorithm to both depend only on the sparsity level k , and not on the ambient dimension n . (The sample complexity is the sketch size m .) We note that the signal vectors can be recovered only up to a sign ambiguity as the pair $(\mathbf{u}_i, \mathbf{v}_i)$ cannot be distinguished from $(-\mathbf{u}_i, -\mathbf{v}_i)$. Furthermore, if there are repeated eigenvalues or singular values, the corresponding signal vectors are recovered up to any rotations within the subspace they span.

Simultaneously sparse and low-rank matrices arise in applications such as sparse PCA [7, 8], sparse bilinear inverse problems [9], community detection [10] and biclustering [11, 12]. In particular, the adjacency matrices of graphs with community structures such as social networks and protein interaction datasets are symmetric, sparse and block-diagonal in appropriate bases [13]. In biclustering, the sample-variable associations in high dimensional data, like gene expression microarray datasets, often correspond to sparse non-overlapping submatrices (or biclusters) in the data matrix.

1.1 Main contributions

Our sketching operator is defined via a combination of a sparse parity check matrix and a partial DFT matrix. This operator was proposed for compressed sensing of (vector) signals in [1, 2]. The sparsity and DFT structure of the operator ensure that the cost of computing the sketch is low. Our main contribution is the design and analysis of a two-stage iterative algorithm to recover the signal vectors from the sketch \mathbf{y} . The two stages use the sparsity and low-rank properties of the signal matrix \mathbf{X}_0 to iteratively identify and solve equations with a single unknown.

Noiseless setting The sketching scheme and the recovery algorithm are described in Section 2 for the noiseless case, that is, when $\mathbf{W} = 0$ in (2). In Section 3, we provide theoretical guarantees on the performance of the scheme. For sufficiently large k , Theorem 1 shows that the scheme has the following features when \mathbf{X}_0 is symmetric in (3):

- 1) When the supports of the signal vectors $\{\mathbf{v}_i\}$ are disjoint, fix any $\delta \in (0, 1)$, with probability at least $1 - 2r \exp(-\frac{1}{30}k^{1-\delta})$, the algorithm recovers the signal vectors with sample complexity $m = 3rk^2/(\delta \ln k)$ and running time $\mathcal{O}(rk^2/\ln k)$. Though this result does not assume any randomness of the signal vectors, we note that with $k = \mathcal{O}(n^\nu)$ for $\nu \in (0, \frac{1}{2})$, and the support locations of each \mathbf{v}_i uniformly random, the supports of the $\{\mathbf{v}_i\}$ will be disjoint with probability at least $1 - 3r^2k^2/n$.
- 2) For the general case, where the supports of the signal vectors are not disjoint, with probability at least $1 - \mathcal{O}(k^{-2})$, the algorithm recovers the signal vectors with sample complexity $m = 2rk^2$ and running time $\mathcal{O}((rk)^3)$.

Theorem 2 provides similar guarantees when \mathbf{X}_0 is non-symmetric as defined in (3). The numerical simulations in Section 3.4 validate the theoretical guarantees. The probabilistic statements in Theorems 1 and 2 are with respect to the randomness in the sketching operator \mathcal{A} , and hold for any rank- r matrix with k -sparse singular vectors.

Near-optimal sample complexity: In the symmetric case, with r orthonormal eigenvectors $\{\mathbf{v}_i\}$, each k -sparse, even if the locations of the nonzeros in $\{\mathbf{v}_i\}$ are known, the degrees of freedom in the eigendecomposition of \mathbf{X}_0 is close to rk . In the non-symmetric case, the degrees of freedom in the singular value decomposition of \mathbf{X}_0 is close to $2r(k - \frac{1}{2})$. Therefore the sample complexity of the proposed scheme is larger than the degrees of freedom by a factor of at most $\mathcal{O}(k)$. Moreover, neither the sample complexity or the running time depends on the ambient dimension n .

Noisy setting The sketching scheme and recovery algorithm are extended to the noisy case in Section 4 (i.e., when $\mathbf{W} \neq 0$ in (2)). Here, the sample complexity is $\mathcal{O}(rk^2 \log(n/k))$, a factor of $\mathcal{O}(\log(n/k))$ greater than that in the noiseless case. This is because additional sketches are needed to reliably identify the locations of nonzero matrix entries in the presence of noise. This also increases the running time of the recovery algorithm to $\mathcal{O}(\max\{n^2 \log(n/k), (rk)^3\})$. We do not provide theoretical performance guarantees in the noisy setting, but show via numerical simulations that the scheme is robust to moderate levels of noise.

1.2 Related work

The sketching operator we use was proposed in [1,2] for compressed sensing of vectors. Variations of the operator have been used for numerous applications including sparse DFT [14,15], sparse Walsh-Hadamard Transform [16–18], compressive phase retrieval [19,20], sparse covariance estimation [21], sparse polynomial learning and graph sketching [22], and learning mixtures of sparse linear regressions [23].

The two-stage recovery algorithm we propose is analogous to the peeling decoder for Low Density Parity Check (LDPC) codes over an erasure channel [24,25], and the first stage of the algorithm is similar to the one used for compressed sensing in [1,2]. However, a key difference from these works is that our sketching matrix has row weights that scale with the sparsity level k and therefore, the existing peeling decoder analysis based on density evolution and Doob Martingales cannot be applied. We characterize the performance of the algorithm by obtaining nonasymptotic probability bounds on the number of unknown nonzero entries after each stage. For the first stage, this is done by establishing negative association (defined in Section 5.1) between the right node degrees in the associated bipartite graph, and using concentration inequalities for negatively associated random

variables [26]. To the best of our knowledge, this technique has not been used previously in the sparse-graph codes literature. For the second stage, we model the algorithm as a random graph process on another bipartite graph, and we analyze an alternative random graph process whose evolution is easier to characterize than the original one.

Other related work: Recovering low-rank matrices from linear measurements (without sparsity constraints) has been widely studied in the past decade; see [27] for an overview. A key result in this area is that if the linear measurement operator satisfies a matrix restricted isometry property, then the low-rank matrix can be recovered via nuclear-norm minimization [28, 29]. For matrices that are simultaneously low-rank and sparse (with $k = o(n)$), such optimization-based approaches are highly sub-optimal with respect to sample complexity.

Several authors have investigated sketching schemes for sparse matrices [30, 31], and simultaneously sparse and low-rank matrices [6, 9, 32, 33]. Moreover, [34, 35] studied the related problem of recovering a sparse low-rank covariance matrix from rank-1 sketches of a sample covariance (the sketching matrices $\mathbf{A}_1, \dots, \mathbf{A}_m$ are rank-1). The recovery algorithms in all these works are based on convex or non-convex optimization, and have running time polynomial in n . The sample complexity also depends at least logarithmically on n . The signal models considered in the works vary, some noise-free and others with additive noise. We refer the reader to Table 1 (noiseless case) and Table 2 (noisy case) for a summary of existing works in comparison to our work.

Reference	Model Assumption	Algorithm	Sample (m)	Time
[32, Thm. 3(a1)]	Sparse & LR	Convex opt.	$\Omega(rn)$	-
[34, Thm. 4]	Sparse & rank-1, symm.	Convex opt.	$\mathcal{O}(k^2 \log n)$	-
[21, Thm. 1]	Sparse only, PSD	MP	$\mathcal{O}(rk^2)$	$\mathcal{O}(rk^2)$
[36, Thm. 1.1]	Rank-1 only, symm.	Convex opt.	$\mathcal{O}(n \log n)$	-
[31, Thm. 1]	Sparse only	Convex opt.	$\mathcal{O}(kn \log^2 n)$	-
Our Thm. 1 & 2 part 1)	Sparse & LR, disjoint supp.	MP	$\mathcal{O}(rk^2 / \log k)$	$\mathcal{O}(rk^2 / \log k)$
Our Thm. 1 & 2 part 2)	Sparse & LR, overlapping supp.	MP	$\mathcal{O}(rk^2)$	$\mathcal{O}((rk)^3)$

Table 1: Comparison of our sketching scheme with existing works on low-rank (LR) and/or sparse matrix recovery. The signal matrix $\mathbf{X} \in \mathbb{R}^{n \times n}$ has rank r , with k -sparse singular vectors. “MP” denotes message passing, and the dashes indicate unreported results. The running time of convex optimization programs is typically $\mathcal{O}(\text{poly}(n))$.

Reference	Model Assumption	Algorithm	Sample (m)	Time
[35, Thm. 1] [33, Thm. 3]	Sparse & LR, PSD	Convex opt.	$\mathcal{O}(rk \log(n/k))$	-
[9, Thm. 6]	Sparse & LR	Non-convex opt.	$\mathcal{O}(rk \log(n/k))$	$\mathcal{O}(rkn^2)$
[34, Thm. 4]	Sparse & rank-1, symm.	Convex opt.	$\mathcal{O}(n^2 \log n)$	-
[21, Thm. 3]	Sparse only, PSD	MP	$\mathcal{O}(rk^2 \log^2 n)$	-
[29, Thm. 2.3]	LR only	Convex opt.	$\mathcal{O}(rn)$	-
[30, Sec. 2]	Sparse only (same as [31])	Convex opt.	-	$\mathcal{O}(n^3)$
Our scheme	Sparse & LR	MP	$\mathcal{O}(rk^2 \log(n/k))$	$\mathcal{O}(n^2 \log(n/k))$

Table 2: Comparison of our scheme with existing works on low-rank (LR) and/or sparse matrix recovery in the noisy case, i.e., the signal matrix is $\mathbf{X} = \mathbf{X}_0 + \mathbf{W}$ where $\mathbf{X}_0 \in \mathbb{R}^{n \times n}$ has rank r , with k -sparse singular vectors.

We remark that our scheme is similar in spirit to the algorithm in [33, 35], which exploits the

sparsity and low-rank structure in different stages. The scheme in [33, 35] uses a nested linear sketching operator, with one part being a restricted isometry for low-rank matrices and the other a restricted isometry for sparse matrices. The recovery algorithm, based on convex programming, correspondingly has two stages, one for low-rank estimation and the other sparse estimation. The sample complexity of the scheme is $\mathcal{O}(rk \log(n/k))$ which is similar to the $\mathcal{O}(rk^2 \log(n/k))$ required by our scheme in the noisy setting. However the recovery algorithm is less robust to noise and significantly slower than ours, as evidenced by the numerical experiments in Section 4.4.1.

The problem of estimating sparse eigenvectors has also been widely studied in the context of sparse PCA [7, 37–39]. In these works, the principal eigenvector of the population covariance matrix is assumed to be sparse. The goal is to recover the principal eigenvector from the sample covariance matrix. This is distinct from the sketching problem considered here.

Some bilinear inverse problems such as phase retrieval [36] and blind deconvolution [40] can be linearized by lifting. That is, they can be reformulated into problems of recovering a rank-1 signal matrix from linear measurements. This is equivalent to low-rank matrix recovery in the rank-1 case, but is different for higher rank. Moreover, the structure of the linear operator in these problems is constrained by the applications, whereas the operator in our setting can be designed flexibly.

1.3 Notation

We write $[n]$ for the set of integers $\{1, 2, \dots, n\}$, \mathbb{N}_0 for $\{0, 1, 2, \dots\}$, and use i to denote $\sqrt{-1}$. For a length- n vector \mathbf{u} , we denote the set of nonzero locations by $\text{supp}(\mathbf{u}) := \{\ell \in [n] : u[\ell] \neq 0\}$. The notation $x_n = o(n^c)$ is used to denote a positive number x_n such that $\frac{x_n}{n^c} \rightarrow 0$ as $n \rightarrow \infty$.

The Bernoulli distribution with parameter $p \in [0, 1]$ is denoted by $\text{Bern}(p)$, and the Binomial distribution with parameters $n \in \mathbb{N}$ and $p \in [0, 1]$ is denoted by $\text{Bin}(n, p)$. $\text{Pois}(\lambda)$ denotes a Poisson distribution with parameter $\lambda > 0$.

2 Baseline sketching scheme and recovery algorithm

We first focus on the noiseless symmetric case in Sections 2.1–2.3, and then extend the scheme to non-symmetric matrices in Section 2.4. The noisy setting is discussed in Section 4.

2.1 Sketching scheme

Consider the noiseless symmetric sparse, low-rank matrix $\mathbf{X} = \sum_{i=1}^r \lambda_i \mathbf{v}_i \mathbf{v}_i^T$ in (2). Let $\tilde{n} = \binom{n}{2} + n$, and let $\mathbf{x} \in \mathbb{R}^{\tilde{n}}$ be the vectorized upper-triangular part of \mathbf{X} . The sketch is $\mathbf{y} = \mathbf{B}\mathbf{x}$, with the sketching matrix $\mathbf{B} \in \mathbb{C}^{2R \times \tilde{n}}$ described below. The sample complexity is $m = 2R$ with the exact value of $R = \mathcal{O}(rk^2 / \ln k)$ given in Theorem 1. We emphasize that vectorizing the signal matrix is just a way of explaining the scheme that makes the notation and analysis in the sequel cleaner.

The sketching matrix $\mathbf{B} \in \mathbb{C}^{2R \times \tilde{n}}$ is constructed as in [1] by taking the column-wise Kronecker product of two matrices: a sparse parity check matrix

$$\mathbf{H} := [\mathbf{h}_1 \quad \mathbf{h}_2 \quad \dots \quad \mathbf{h}_{\tilde{n}}] \in \{0, 1\}^{R \times \tilde{n}}, \quad (4)$$

and a matrix \mathbf{S} consisting of the first two rows of an \tilde{n} -point DFT matrix:

$$\mathbf{S} := \begin{bmatrix} 1 & 1 & 1 & \dots & 1 \\ 1 & W & W^2 & \dots & W^{\tilde{n}-1} \end{bmatrix} \quad \text{where } W = \exp\left(\frac{2\pi i}{\tilde{n}}\right). \quad (5)$$

Then,

$$\mathbf{B} := \left[\mathbf{h}_1 \otimes \begin{bmatrix} 1 \\ 1 \end{bmatrix} \quad \mathbf{h}_2 \otimes \begin{bmatrix} 1 \\ W \end{bmatrix} \quad \dots \quad \mathbf{h}_{\tilde{n}} \otimes \begin{bmatrix} 1 \\ W^{\tilde{n}-1} \end{bmatrix} \right]. \quad (6)$$

For column vectors \mathbf{a}, \mathbf{b} with lengths n_a, n_b , we recall that the Kronecker product $\mathbf{a} \otimes \mathbf{b}$ is the length- $(n_a + n_b)$ vector $[a_1 \mathbf{b}^T, a_2 \mathbf{b}^T, \dots, a_{n_a} \mathbf{b}^T]^T$. As an example, let $\tilde{n} = 6$, $R = 4$ and

$$\mathbf{H} = \begin{bmatrix} 1 & 1 & 1 & 0 & 1 & 1 \\ 0 & 0 & 0 & 1 & 1 & 1 \\ 1 & 0 & 0 & 0 & 0 & 0 \\ 0 & 1 & 1 & 1 & 0 & 0 \end{bmatrix}, \quad \mathbf{S} = \begin{bmatrix} 1 & 1 & \dots & 1 \\ 1 & W & \dots & W^5 \end{bmatrix}. \quad (7)$$

Then the sketching matrix \mathbf{B} is

$$\mathbf{B} = \begin{bmatrix} 1 & 1 & 1 & 0 & 1 & 1 \\ 1 & W & W^2 & 0 & W^4 & W^5 \\ 0 & 0 & 0 & 1 & 1 & 1 \\ 0 & 0 & 0 & W^3 & W^4 & W^5 \\ 1 & 0 & 0 & 0 & 0 & 0 \\ 1 & 0 & 0 & 0 & 0 & 0 \\ 0 & 1 & 1 & 1 & 0 & 0 \\ 0 & W & W^2 & W^3 & 0 & 0 \end{bmatrix}. \quad (8)$$

We choose \mathbf{H} to be column-regular, with each column containing $d \geq 2$ ones at locations chosen uniformly at random; the example in (7) uses $d = 2$. The sparse matrix \mathbf{H} determines which nonzero entries of \mathbf{x} contribute to each entry of the sketch \mathbf{y} .

It is convenient to view the sketch $\mathbf{y} = \mathbf{B}\mathbf{x} \in \mathbb{C}^{2R}$ as having R pairs of entries. We denote the j -th pair $[y_{(2j-1)}, y_{(2j)}]^T$ by $\mathbf{y}_j \in \mathbb{C}^2$ and call it the j -th sketch *bin*. Let $\mathbf{B}_j \in \mathbb{C}^{2 \times \tilde{n}}$ denote the matrix containing the j -th pair of rows in \mathbf{B} , for $j \in [R]$. We observe that the j -th bin can be expressed as

$$\mathbf{y}_j = \mathbf{B}_j \mathbf{x} = \mathbf{S} \mathbf{x}_j^*, \quad (9)$$

where the entries of $\mathbf{x}_j^* \in \mathbb{R}^{\tilde{n}}$ are

$$(x_j^*)_\ell = \begin{cases} x_\ell & \ell \in \mathcal{N}(j) \\ 0 & \ell \notin \mathcal{N}(j) \end{cases} \quad \text{for } \ell \in [\tilde{n}]. \quad (10)$$

Here, $\mathcal{N}(j) := \{\ell \in [\tilde{n}] : H_{j,\ell} = 1\}$ contains the locations of the ones in the j -th row of \mathbf{H} . In words, (9) shows that the bin \mathbf{y}_j is a linear combination of the \mathbf{x} entries that correspond to the ones in the j -th row of \mathbf{H} . Specifically, \mathbf{y}_j is the sum of these \mathbf{x} entries, weighted by their respective columns in \mathbf{S} . Note that (9) can be recast into two equations in the form of (1), one for each component in the bin \mathbf{y}_j . Moreover, when only one nonzero \mathbf{x} entry contributes to \mathbf{y}_j , the DFT structure of \mathbf{S} enables exact recovery of that nonzero from \mathbf{y}_j .

2.2 Recovery algorithm for rank-1 symmetric matrices

For ease of exposition, we first describe the recovery algorithm for rank-1 matrices (i.e., $\mathbf{X} = \lambda \mathbf{v} \mathbf{v}^T$), and then explain how to extend the algorithm to tackle rank- r matrices. The algorithm has two stages, which we refer to as stage A and stage B.

- In stage A, by exploiting the sparsity of \mathbf{X} , the algorithm iteratively recovers as many of the nonzero entries in \mathbf{X} as possible from the sketch \mathbf{y} . This stage is similar to the compressed sensing recovery algorithm used in [1,2]. For sufficiently large k , stage A recovers at least one nonzero diagonal entry and a fraction $k^{-\delta}$ of the nonzero above-diagonal entries in \mathbf{X} with high probability, for a constant $\delta \in (0, 1)$.
- In stage B, by exploiting the rank-1 structure of \mathbf{X} , the algorithm iteratively recovers the nonzero entries in \mathbf{v} from the partially recovered matrix \mathbf{X} . Theorem 1 shows that with a sketch of size $3k^2/\ln k$, the algorithm recovers \mathbf{v} by the end of stage B with high probability, for sufficiently large k .

We note that the recovery algorithm does not require knowledge of the sparsity k .

2.2.1 Stage A of the algorithm

Following the terminology in [1], we classify each of the R bins of \mathbf{y} based on how many nonzero entries of \mathbf{X} contribute to the pair of linear combinations defining the bin. Specifically, a bin \mathbf{y}_j is referred to as a *zeroton*, *singleton*, or *multiton* respectively if it involves zero, one, or more than one nonzero entries of \mathbf{X} , that is, when $|\text{supp}(\mathbf{x}) \cap \mathcal{N}(j)| = 0, 1$ or > 1 with $\mathcal{N}(j)$ as defined in (10). This is illustrated by the following example with the sketching matrix \mathbf{B} in (8):

$$\begin{array}{c}
 \mathbf{y} \in \mathbb{C}^{2R} \\
 \mathbf{y}_1 \\
 \mathbf{y}_2 \\
 \mathbf{y}_3 \\
 \mathbf{y}_4
 \end{array}
 =
 \begin{array}{c}
 \mathbf{B} \in \mathbb{C}^{2R \times \tilde{n}} \\
 \begin{bmatrix}
 \blacksquare & \blacksquare & \blacksquare & \square & \blacksquare & \blacksquare \\
 \blacksquare & \blacksquare & \blacksquare & \square & \blacksquare & \blacksquare \\
 \square & \square & \square & \blacksquare & \blacksquare & \blacksquare \\
 \square & \square & \square & \blacksquare & \blacksquare & \blacksquare \\
 \blacksquare & \square & \square & \square & \square & \square \\
 \blacksquare & \square & \square & \square & \square & \square \\
 \square & \blacksquare & \blacksquare & \blacksquare & \square & \square \\
 \square & \blacksquare & \blacksquare & \blacksquare & \square & \square
 \end{bmatrix}
 \end{array}
 \begin{array}{c}
 \mathbf{x} \in \mathbb{R}^{\tilde{n}} \\
 \begin{bmatrix}
 \square \\
 \color{red}\square \\
 \color{blue}\square \\
 \square \\
 \square \\
 \square \\
 \color{red}\square \\
 \color{blue}\square
 \end{bmatrix}
 \begin{array}{l}
 x_1 \equiv X_{11} \\
 x_2 \equiv X_{12} \\
 x_3 \equiv X_{13} \\
 x_4 \equiv X_{22} \\
 x_5 \equiv X_{23} \\
 x_6 \equiv X_{33}
 \end{array}
 \end{array}
 .$$

The white squares (\square) represent zeros, and the black squares (\blacksquare) represent the DFT coefficients in \mathbf{B} . The coloured squares in \mathbf{x} represent the nonzero entries. The sketch \mathbf{y} consists of $R = 4$ bins, of which \mathbf{y}_3 (\square) is a zeroton, \mathbf{y}_2 ($\color{blue}\square$) is a singleton, and \mathbf{y}_1 ($\color{red}\square$) and \mathbf{y}_4 ($\color{blue}\square$) are multitons.

The first step is to classify each bin \mathbf{y}_j into one of the three types. For brevity, we denote the two components of \mathbf{y}_j as $y_{(2j-1)}$ and $y_{(2j)}$. If both $y_{(2j-1)}$ and $y_{(2j)}$ are zero, then \mathbf{y}_j is declared a zeroton. This is because the DFT coefficients in \mathbf{B} ensure that $y_{(2j)}$ can be zero only when the \mathbf{x} entries involved in the linear combination are all zero, i.e., $\text{supp}(\mathbf{x}) \cap \mathcal{N}(j) = \emptyset$. Next, to identify singletons, (9) and (10) indicate that a singleton takes the form

$$\mathbf{y}_j = \begin{bmatrix} y_{(2j-1)} \\ y_{(2j)} \end{bmatrix} = x_\ell \begin{bmatrix} 1 \\ W^{\ell-1} \end{bmatrix}, \quad (11)$$

where x_ℓ is the sole nonzero entry contributing to the bin \mathbf{y}_j , i.e., $\text{supp}(\mathbf{x}) \cap \mathcal{N}(j) = \ell$. While $y_{(2j-1)}$ directly captures the value of x_ℓ , the components $y_{(2j-1)}$ and $y_{(2j)}$ together capture the location ℓ . Therefore, to identify a singleton, the algorithm computes

$$\hat{\ell} = \frac{\arg \{y_{(2j)}/y_{(2j-1)}\}}{2\pi/\tilde{n}} + 1, \quad \hat{x}_\ell = y_{(2j-1)}. \quad (12)$$

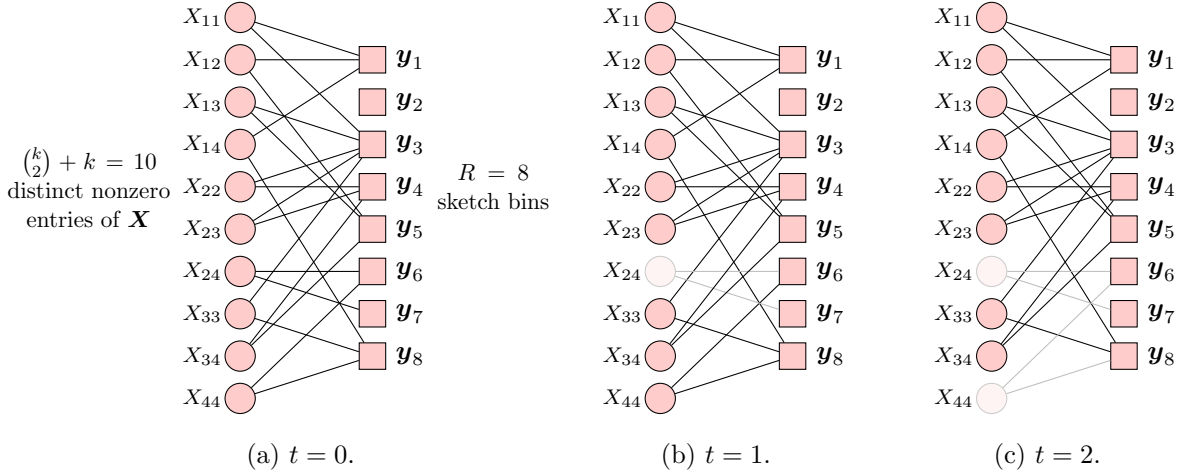


Figure 1: (a): Pruned bipartite graph for stage A corresponding to $\mathbf{H} \in \{0, 1\}^{R \times \tilde{n}}$. Here, $\mathbf{X} = \lambda \mathbf{v} \mathbf{v}^T$ with $v_i \neq 0$ for $i \in [4]$ and $v_i = 0$ for $5 \leq i \leq n$, and $R = 8$. (b)–(c): The graph process that models the recovery of the nonzero entries of \mathbf{X} . The faded nodes and edges are those that have been peeled off.

If $|y_{(2j-1)}| = |y_{(2j)}|$ and the estimated index $\hat{\ell}$ takes an integer value in $[\tilde{n}]$, the algorithm declares \mathbf{y}_j a singleton and the $\hat{\ell}$ -th entry of \mathbf{x} as $\hat{x}_{\hat{\ell}}$. The algorithm declares \mathbf{y}_j a multiton if it is found to be neither a zero-ton nor a singleton.

Note that when the target signal matrix is complex-valued, the linear measurements in a bin may be all-zero even when the matrix entries involved in the bin are not all zeros. Therefore, one way to tackle complex signal matrices would be to measure and recover their real and imaginary parts separately using the proposed scheme.

Let $t \in \mathbb{N}_0$ denote the iteration number and let $\mathcal{S}(t)$ be the set of singletons at time t . At $t = 0$, the algorithm identifies the initial set of singletons $\mathcal{S}(0)$ among the R bins. Then at each $t \geq 1$, the algorithm picks a singleton uniformly at random from $\mathcal{S}(t-1)$, and recovers the support of \mathbf{x} underlying the singleton using the index-value pair $(\hat{\ell}, \hat{x}_{\hat{\ell}})$ in (12). The algorithm then subtracts (or ‘peels off’) the contribution of the $\hat{\ell}$ -th entry of \mathbf{x} from each of the d bins the entry is involved in, re-categorizes these bins, and updates the set of singletons to include any new singletons created by the peeling of the $\hat{\ell}$ -th entry. The updated set is $\mathcal{S}(t)$. The algorithm continues until singletons run out, i.e., when $\mathcal{S}(t) = \emptyset$. The pseudocode for stage A is provided in Algorithm 1 below, with line 11 providing the formula for each peeling step.

It is useful to visualize the peeling algorithm using a bipartite graph constructed from the parity check matrix $\mathbf{H} \in \{0, 1\}^{R \times \tilde{n}}$ (which was used to define the sketching matrix \mathbf{B}). As shown in Fig. 1a, the $\tilde{k} = \binom{k}{2} + k$ left nodes correspond to the unknown nonzero entries in \mathbf{X} at $t = 0$, and the R right nodes correspond to the bins. Each left node connects to d distinct right nodes. The left nodes connected to each right node (bin) are those that appear in the linear constraints defining the bin. We call Fig. 1a a ‘pruned’ graph as we have removed the left nodes detected to be zeros (via zero-ton bins). As illustrated in Figs. 1b and 1c, the algorithm first recovers and peels off X_{24} from the singleton \mathbf{y}_7 at $t = 1$. This creates a singleton \mathbf{y}_6 from which X_{44} is recovered and peeled off at $t = 2$. The algorithm terminates at $t = 2$ as there are no more singletons.

Algorithm 1 Peeling decoder in stage A

INPUT: sketch vector $\mathbf{y} \in \mathbb{C}^{2R}$, coding matrix $\mathbf{H} \in \{0, 1\}^{R \times \tilde{n}}$.OUTPUT: an estimate of the vectorized signal matrix $\hat{\mathbf{x}} \in \mathbb{R}^{\tilde{n}}$.

```
1: Initialize:  $\hat{\mathbf{x}} \leftarrow \mathbf{0}_{\tilde{n}}$ ,  $\mathcal{R} \leftarrow \{1, 2, \dots, R\}$ . ▷  $\mathcal{R}$ : set of right nodes to be checked
2: while  $\mathcal{R} \neq \emptyset$  do
3:    $\mathcal{R}' \leftarrow \mathcal{R}$  ▷  $\mathcal{R}'$ : right nodes to be checked in the next iteration
4:   for each  $j \in \mathcal{R}$  do
5:     if  $\mathbf{y}_j$  is a zero-ton then
6:        $\mathcal{R}' \leftarrow \mathcal{R}' \setminus j$ 
7:     else if  $\mathbf{y}_j$  is a singleton (determined via (12)) then
8:       recover the  $\hat{\ell}$ -th entry of  $\hat{\mathbf{x}}$  as  $\hat{x}_{\hat{\ell}}$  according to (12)
9:        $\mathcal{C} \leftarrow \{i \in [R] : H_{i\hat{\ell}} = 1\}$ 
10:      for each  $i \in \mathcal{C}$  do ▷ peel off connecting right nodes
11:         $\mathbf{y}_i \leftarrow \mathbf{y}_i - \hat{x}_{\hat{\ell}} \begin{bmatrix} 1 \\ \exp(2\pi i(\hat{\ell} - 1)/\tilde{n}) \end{bmatrix}$ 
12:      end for
13:       $\mathcal{R}' \leftarrow \mathcal{R}' \cup \mathcal{C} \setminus j$ 
14:    else
15:       $\mathcal{R}' \leftarrow \mathcal{R}' \setminus j$ 
16:    end if
17:  end for
18:   $\mathcal{R} \leftarrow \mathcal{R}'$ 
19: end while
20: return  $\hat{\mathbf{x}}$ 
```

2.2.2 Stage B of the algorithm

Recalling that $\mathbf{X} = \lambda \mathbf{v} \mathbf{v}^T$, we write $\tilde{\mathbf{v}} := \sqrt{|\lambda|} \mathbf{v}$ for the unsigned, unnormalized eigenvector. Stage B of the algorithm uses the rank-1 structure of \mathbf{X} to recover the nonzeros in $\tilde{\mathbf{v}}$ from the nonzero entries of \mathbf{X} that were recovered in stage A. When fully recovered, $\tilde{\mathbf{v}}$ is normalized to give \mathbf{v} . Since the j -th diagonal entry of \mathbf{X} is λv_j^2 , the sign of λ can be determined from any nonzero diagonal entry recovered in stage A. We now describe stage B for $\lambda > 0$, and then explain the small adjustment needed for $\lambda < 0$.

Since \mathbf{X} is rank-1, its $\binom{k}{2}$ nonzero above-diagonal entries are pairwise products of the form $\tilde{v}_i \tilde{v}_j$. The proof of Theorem 1 shows that in stage A, with high probability, at least a fraction $k^{-\delta}$ of these pairwise products are recovered, for a constant $\delta \in (0, 1)$. (See Lemma 3.1). Stage B of the algorithm can be visualized using another bipartite graph shown in Fig. 2a. The k left nodes represent the unknown nonzero entries in $\tilde{\mathbf{v}}$, and the right nodes represent the nonzero pairwise products in \mathbf{X} recovered in stage A. The right nodes are the product constraints that the left nodes satisfy. This is a pruned graph because any zero entries in $\tilde{\mathbf{v}}$ or \mathbf{X} have been excluded from the graph.

At $t = 0$, the algorithm picks one of the nonzero diagonal entries recovered in stage A, say X_{jj} , and declares $\sqrt{X_{jj}}$ as the value of the left node \tilde{v}_j . The algorithm then removes (peels off) the contribution of \tilde{v}_j from the right nodes that \tilde{v}_j connects to by dividing these right nodes by $\sqrt{X_{jj}}$. Fig. 2b shows this initial step with \tilde{v}_4 being a left node whose squared value was recovered

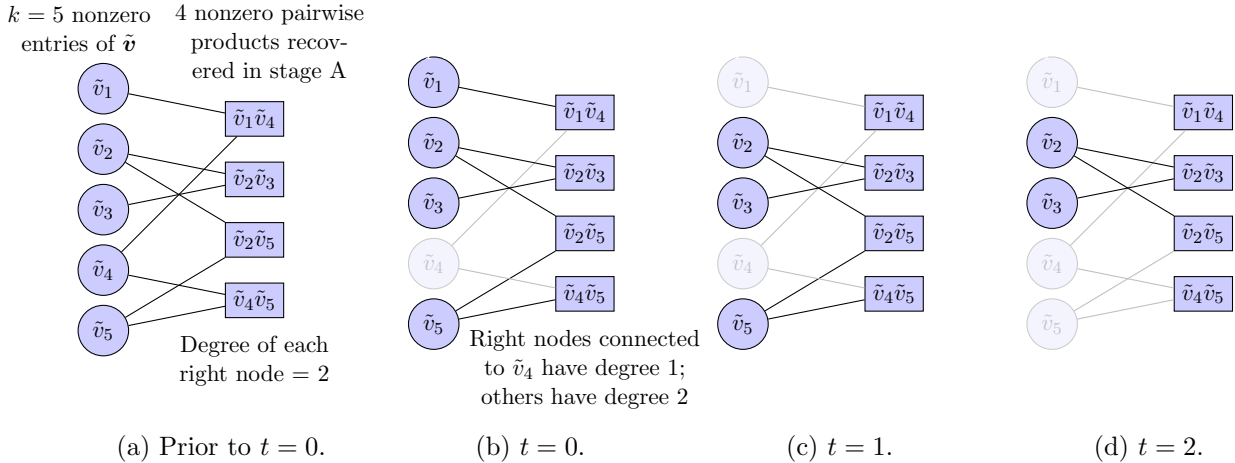


Figure 2: (a): Pruned bipartite graph for stage B with $\mathbf{X} = \tilde{\mathbf{v}}\tilde{\mathbf{v}}^T$, where $\tilde{v}_i \neq 0$ for $i \in [5]$ and $\tilde{v}_i = 0$ for $6 \leq i \leq n$. (b)–(d): The graph process that models the recovery of the nonzero entries in $\tilde{\mathbf{v}}$ from the nonzero matrix entries recovered in stage A. The faded nodes and edges are those that have been peeled off. At $t = 0$, the left node \tilde{v}_4 is peeled off based on the recovered nonzero diagonal entry X_{44} .

in stage A and is peeled off at $t = 0$. Once the first left node is peeled off, all of its connecting right nodes reduce from degree-2 nodes to degree-1. For $t \geq 1$, the algorithm proceeds similarly to stage A, noting that in stage B, each right node represents the product of its two connecting left nodes rather than a linear combination. At each step, a degree-1 right node is picked uniformly at random from the available ones and its connecting left node recovered and peeled off to update the set of degree-1 right nodes. The algorithm continues until there are no more degree-1 right nodes. All the unrecovered entries of $\tilde{\mathbf{v}}$ are set to zero. In Fig. 2c and 2d, the left nodes \tilde{v}_1 and \tilde{v}_5 are recovered via $\tilde{v}_1\tilde{v}_4$ and $\tilde{v}_4\tilde{v}_5$, respectively, and peeled off. Moreover, \tilde{v}_2 and \tilde{v}_3 can be recovered via $\tilde{v}_2\tilde{v}_5$ and $\tilde{v}_2\tilde{v}_3$ before degree-1 right nodes run out. The pseudocode for stage B is provided in Algorithm 2 below, which calls the subroutine `recover_eigenvect` defined in Algorithm 3.

The $\lambda < 0$ case We flip the sign of each right node (pairwise product) before running stage B of the algorithm as above to recover $\tilde{\mathbf{v}} = \sqrt{|\lambda|}\mathbf{v}$. See lines 4–9 of Algorithm 3 for the pseudocode of this operation.

2.3 Recovery algorithm for rank- r symmetric matrices

Disjoint supports When the eigenvectors $\{\mathbf{v}_i\}$ are known to have disjoint supports, the same two-stage algorithm can be used. The only difference is that the graphical representation for stage B (Fig. 2a) will now consist of r disjoint bipartite graphs. For each of these graphs, stage B of the algorithm is initialized using a nonzero diagonal entry recovered in stage A. See Algorithm 2 below for details.

General case When the supports of the r eigenvectors have overlaps, we cannot use stage B of the algorithm as it depends on the entries of \mathbf{X} being pairwise products of the eigenvector entries. We therefore take a large enough sketch to identify all the nonzero entries in \mathbf{X} in stage A. This

Algorithm 2 Peeling decoder in stage B (for rank- r symmetric matrices)

INPUT: partially recovered signal matrix $\hat{\mathbf{X}} \in \mathbb{R}^{n \times n}$, the rank r .OUTPUT: an estimate of the unnormalized eigenvectors $\tilde{\mathbf{v}}_1, \tilde{\mathbf{v}}_2, \dots, \tilde{\mathbf{v}}_r \in \mathbb{R}^n$.**Require:** the true signal matrix \mathbf{X} is symmetric rank- r with eigenvectors having disjoint supports.

- 1: **Initialize:** $\tilde{\mathbf{v}}_1, \tilde{\mathbf{v}}_2, \dots, \tilde{\mathbf{v}}_r \leftarrow \mathbf{0}_n$
 - 2: $\mathcal{S} \leftarrow \{i \in [n] : \hat{X}_{ij} \neq 0 \text{ for any } j \in [n]\}, \hat{k} \leftarrow |\mathcal{S}|$
 - 3: $\hat{\mathbf{X}}^s \leftarrow \hat{\mathbf{X}}_{\mathcal{S}, \mathcal{S}}$ ▷ extract nonzero submatrix to process
 - 4: **for** $i = 1$ to r **do**
 - 5: $\tilde{\mathbf{v}}_i^s, \hat{\mathbf{X}}^s \leftarrow \text{recover_eigenvec}(\hat{\mathbf{X}}^s)$ ▷ recover one eigenvector and update $\hat{\mathbf{X}}^s$
 - 6: $\tilde{\mathbf{v}}_{i\mathcal{S}} \leftarrow \tilde{\mathbf{v}}_i^s$
 - 7: **end for**
 - 8: **return** $\tilde{\mathbf{v}}_1, \tilde{\mathbf{v}}_2, \dots, \tilde{\mathbf{v}}_r$
-

Algorithm 3 recover_eigenvec: Recovery of one eigenvector for a symmetric matrix

INPUT: partially recovered nonzero submatrix $\hat{\mathbf{X}}^s \in \mathbb{R}^{\hat{k} \times \hat{k}}$ (unrecovered entries stored as zeros).OUTPUT: an estimate of one unnormalized eigenvector $\tilde{\mathbf{v}}^s \in \mathbb{R}^{\hat{k}}$,
 $\hat{\mathbf{X}}^s$ with its entries used to infer $\tilde{\mathbf{v}}^s$ reset to zeros.**Require:** the true signal matrix \mathbf{X} is symmetric rank- r with eigenvectors having disjoint supports.

- 1: **Initialize:** $\tilde{\mathbf{v}}^s \leftarrow \mathbf{0}_{\hat{k}}$
 - 2: **if** $\{i \in [\hat{k}] : \hat{X}_{ii}^s \neq 0\} \neq \emptyset$ **then**
 - 3: $\ell \leftarrow$ an index chosen randomly from $\{i \in [\hat{k}] : \hat{X}_{ii}^s \neq 0\}$
 - 4: **if** $\hat{X}_{\ell\ell}^s > 0$ **then**
 - 5: flip_sign \leftarrow False
 - 6: **else**
 - 7: flip_sign \leftarrow True
 - 8: $\hat{\mathbf{X}}^s \leftarrow -\hat{\mathbf{X}}^s$
 - 9: **end if**
 - 10: $\tilde{\mathbf{v}}^s \leftarrow \tilde{\mathbf{v}}^s + \left[\hat{X}_{1\ell}^s, \hat{X}_{2\ell}^s, \dots, \hat{X}_{\hat{k}\ell}^s \right]^T / \sqrt{\hat{X}_{\ell\ell}^s}$ ▷ peel off ℓ -th left node
 - 11: $\mathcal{I} \leftarrow \{i \in [\hat{k}] : \tilde{v}_i^s \neq 0\}$
 - 12: $\hat{X}_{ij}^s \leftarrow 0 \quad \forall i, j \in \mathcal{I}$
 - 13: $\mathcal{L} \leftarrow \mathcal{I} \setminus \ell$ ▷ \mathcal{L} : set of left nodes connecting to singletons
 - 14: **while** $\mathcal{L} \neq \emptyset$ and $|\mathcal{I}| < \hat{k}$ **do**
 - 15: $\ell \leftarrow$ an index chosen randomly from \mathcal{L}
 - 16: $\tilde{\mathbf{v}}^s \leftarrow \tilde{\mathbf{v}}^s + \left[\hat{X}_{1\ell}^s, \hat{X}_{2\ell}^s, \dots, \hat{X}_{\hat{k}\ell}^s \right]^T / \tilde{v}_\ell^s$ ▷ peel off ℓ -th left node
 - 17: $\mathcal{L} \leftarrow (\mathcal{L} \setminus \ell) \cup \{i \in [\hat{k}] : \hat{X}_{i\ell}^s \neq 0\}$
 - 18: $\mathcal{I} \leftarrow \{i \in [\hat{k}] : \tilde{v}_i^s \neq 0\}$
 - 19: $\hat{X}_{ij}^s \leftarrow 0 \quad \forall i, j \in \mathcal{I}$
 - 20: **end while**
 - 21: **if** flip_sign **then** $\hat{\mathbf{X}}^s \leftarrow -\hat{\mathbf{X}}^s$
 - 22: **end if**
 - 23: **end if**
 - 24: **return** $\tilde{\mathbf{v}}^s, \hat{\mathbf{X}}^s$
-

is equivalent to compressed sensing recovery of the complete vectorized matrix using the scheme of [1, 2]. We then perform an eigendecomposition on the recovered submatrix of nonzero entries to obtain the nonzero entries of $\{\mathbf{v}_1, \dots, \mathbf{v}_r\}$. This submatrix has size at most $rk \times rk$, hence the complexity of its eigendecomposition is $\mathcal{O}((rk)^3)$, which does not depend on the ambient dimension n . Recovering the entire matrix \mathbf{X} in stage A requires a sample complexity $m = \mathcal{O}(rk^2)$, which is larger by a factor of $\ln k$ than that needed in the case of disjoint supports.

2.4 Recovery of non-symmetric matrices

Consider the non-symmetric case where \mathbf{X} has the form $\mathbf{X} = \sum_{i=1}^r \sigma_i \mathbf{u}_i \mathbf{v}_i^T$ where $\{\mathbf{u}_i, \mathbf{v}_i\}$ each has at most k nonzero entries. The sketching operator is the same as in the symmetric case, except that here it acts on the entire matrix \mathbf{X} . Consider first the case where the singular vectors $\{\mathbf{u}_i\}$ have disjoint supports as do $\{\mathbf{v}_i\}$. Based on the sketch, stage A of the algorithm can be used to recover a small fraction of the nonzero entries in \mathbf{X} like in the symmetric case. Using the recovered nonzero matrix entries, stage B of the algorithm iteratively recovers the nonzeros in $\{\mathbf{u}_i, \mathbf{v}_i\}$. While stage B can still be viewed as a peeling decoder, the associated bipartite graph has a different structure from the symmetric case. The initialization step is also different.

We take the rank-1 case as an example, where $\mathbf{X} = \sigma \mathbf{u} \mathbf{v}^T$. The peeling algorithm recovers $\tilde{\mathbf{u}}$ and $\tilde{\mathbf{v}}$, which are scaled versions of \mathbf{u} and \mathbf{v} such that $\tilde{\mathbf{u}} \tilde{\mathbf{v}}^T = \mathbf{X}$; these vectors are then normalized to obtain σ, \mathbf{u} and \mathbf{v} . Fig. 3a illustrates the pruned stage B graph in this setting. The left nodes represent the nonzero entries in $\tilde{\mathbf{u}}$ and $\tilde{\mathbf{v}}$, and the right nodes represent the nonzero pairwise products recovered in stage A. Each right node connects to one nonzero in $\tilde{\mathbf{u}}$ and one nonzero in $\tilde{\mathbf{v}}$ and equals the product of these two nonzeros.

Since a non-symmetric matrix has no entries in squared form, the peeling process is initiated by arbitrarily assigning the value 1 to one of the left nodes who have at least one neighbouring right

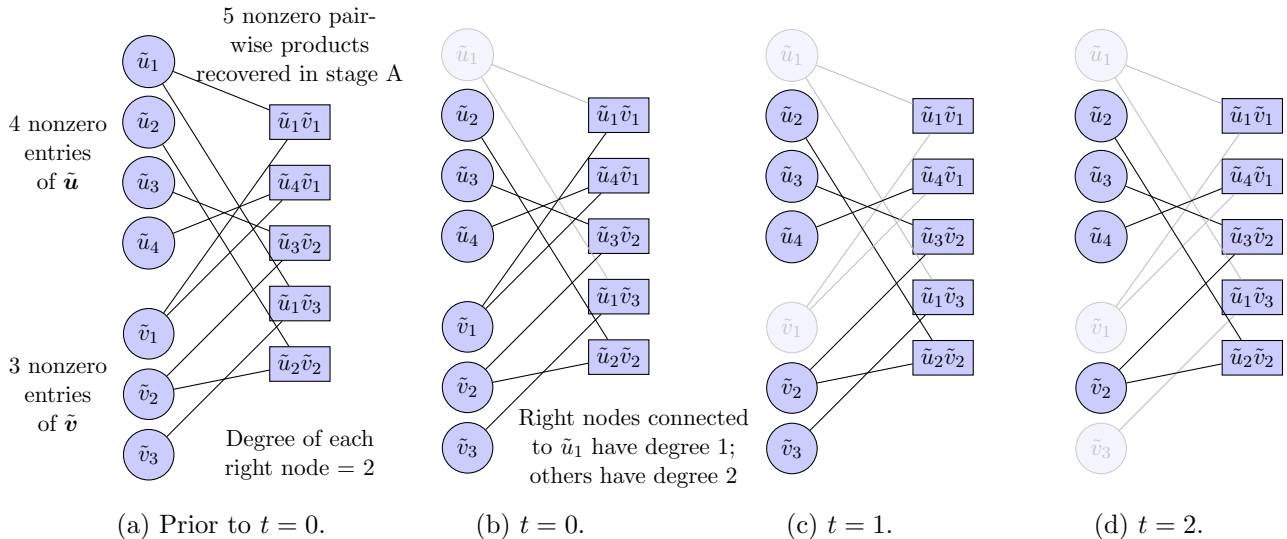


Figure 3: (a): Pruned bipartite graph for stage B when \mathbf{X} is non-symmetric. Here, $\mathbf{X} = \sigma \mathbf{u} \mathbf{v}^T = \tilde{\mathbf{u}} \tilde{\mathbf{v}}^T$ with $\tilde{u}_j \neq 0$ for $j \in [4]$, $\tilde{u}_j = 0$ for $5 \leq j \leq n$, $\tilde{v}_j \neq 0$ for $j \in [3]$ and $\tilde{v}_j = 0$ for $4 \leq j \leq n$. (b)–(d): The graph process that models the recovery of $\tilde{\mathbf{u}}$ and $\tilde{\mathbf{v}}$. At $t = 0$, \tilde{u}_1 is recovered as 1 and peeled off. Following the recovery of \tilde{u}_1 , the left nodes \tilde{v}_1, \tilde{v}_3 (and \tilde{u}_4) can be peeled off too.

node. At $t = 0$, this left node is peeled off from the graph, and its connecting right node then have degree 1. In Fig. 3b, the algorithm recovers \tilde{u}_1 as 1 and peels it off at $t = 0$. This turns the right nodes $\tilde{u}_1\tilde{v}_1$ and $\tilde{u}_1\tilde{v}_3$ from degree-2 into degree-1.

For $t \geq 1$, like in the symmetric case, the algorithm peels one degree-1 right node at a time along with the left node connecting to the right node, until no degree-1 right nodes remain in the graph. In Figs. 3c and 3d, at $t = 1$ and $t = 2$, \tilde{v}_1 and \tilde{v}_3 are recovered and peeled off sequentially.

For rank $r > 1$, when both sets of singular vectors $\{\mathbf{u}_i\}$ and $\{\mathbf{v}_i\}$ have disjoint supports, the bipartite graph for stage B consists of r disjoint subgraphs. The peeling algorithm in this case is equivalent to the rank-1 algorithm run in parallel on the r subgraphs.

For the general case with $r > 1$ and the $\{\mathbf{u}_i\}$ or $\{\mathbf{v}_i\}$ having overlapping supports, like in the symmetric case, we use a large enough sketch such that stage A recovers all the nonzeros in \mathbf{X} . A singular value decomposition on the recovered nonzero submatrix gives the nonzeros in $\{\mathbf{u}_i, \mathbf{v}_i\}$.

3 Main results

Theorem 1 (Noiseless symmetric case). *Consider the matrix $\mathbf{X} = \sum_{i=1}^r \lambda_i \mathbf{v}_i \mathbf{v}_i^T$ where each eigenvector \mathbf{v}_i has k nonzero entries. For sufficiently large k , the sketching scheme with recovery algorithm described in Sections 2.1–2.3 has the following guarantees.*

- 1) *For the case $r = 1$ or $r > 1$ with the supports of $\{\mathbf{v}_i\}$ disjoint, fix $\delta \in (0, 1)$ and let $R = dr\tilde{k}/(\delta \ln k)$. Here, we recall that $\tilde{k} = \binom{k}{2} + k$, and $d \geq 2$ is the number of ones in each column of \mathbf{H} (i.e., the degree of each left node in the pruned stage A bipartite graph).*

Then, with probability at least $1 - 2r \exp(-\frac{1}{30}k^{1-\delta})$, the two-stage algorithm recovers $\{\mathbf{v}_i\}$ (up to a sign ambiguity) from the sketch of size $m = 2R$ with running time $\mathcal{O}(rk^2 / \ln k)$.

- 2) *When $r > 1$ and the supports of $\{\mathbf{v}_i\}$ may overlap, with probability at least $1 - \mathcal{O}(k^{-2})$, stage A of the algorithm followed by eigendecomposition of the recovered nonzero submatrix recovers $\{\mathbf{v}_i\}$ from a sketch of size $m = 3r\tilde{k}$ with running time $\mathcal{O}((rk)^3)$.*

Remarks:

1. The eigenvectors $\{\mathbf{v}_i\}$ can only be recovered up to a sign ambiguity since $\mathbf{v}_i \mathbf{v}_i^T = (-\mathbf{v}_i)(-\mathbf{v}_i)^T$. Moreover, when there is an eigenvalue with multiplicity $m > 1$, the corresponding eigenvectors can only be recovered up to a rotation within the m -dimensional subspace they span.
2. When the eigenvectors have different sparsities $\{k_1, \dots, k_r\}$, Theorem 1 holds with the sample complexity depending on $\max\{k_1, \dots, k_r\}$ and the success probability on $\min\{k_1, \dots, k_r\}$.
3. The probability guarantees are with respect to the randomness in the sketching matrix (specifically, in the locations of the ones in the parity check matrix \mathbf{H}). No randomness assumptions are made on the eigenvectors $\{\mathbf{v}_i\}$, and the result holds for any rank- r matrix with k -sparse eigenvectors.
4. The bound on the success probability in part 1) is not tight. The bound also does not depend d since this parameter appears in a term in the proof that is of a smaller order. In the simulations in Sections 3.4 and 4.4, we use $d = 2$.

5. The upper bound on the failure probability depends only on k . In contrast, conventional sketching schemes using optimization based recovery, e.g. [32], have failure probabilities decaying with n . This is because the sketch size in our scheme depends only on k , and not on the ambient dimension n , unlike the conventional schemes. In practice, the failure probability of our scheme is found to be extremely small even for small values of $\frac{k}{n}$ (where our failure probability is expected to decay slower). See the sharp phase transitions in performance measures in Figs. 4 and 6.
6. In part 1), the first stage of the algorithm is similar to the peeling decoder for LDPC codes over an erasure channel [24,25] and the decoder used for compressed sensing in [1,2]. However, our sketching matrix \mathbf{B} (defined via the parity check matrix \mathbf{H}) has row weights that scale with the sparsity level k . This implies that each iteration of the peeling algorithm can introduce large changes in the degree distribution, which makes it challenging to bound the evolution of the peeling process. Thus the existing peeling decoder analysis based on density evolution and Doob martingales cannot be applied. See comments following Lemma 3.1.

Theorem 2 (Noiseless non-symmetric case). *Consider the matrix $\mathbf{X} = \sum_{i=1}^r \sigma_i \mathbf{u}_i \mathbf{v}_i^T$, where each left singular vector \mathbf{u}_i has k nonzero entries and each right singular vector \mathbf{v}_i has βk nonzero entries, for some constant $\beta \in (0, 1]$. For sufficiently large k , the sketching scheme with recovery algorithm described in Section 2.4 has the following guarantees.*

- 1) *For the case $r = 1$ or $r > 1$ with each set of singular vectors $\{\mathbf{u}_i\}$ and $\{\mathbf{v}_i\}$ having disjoint supports, fix $\delta \in (0, \frac{1}{2})$ and let $R = dr\beta k^2 / (\delta \ln k)$. Then, with probability at least $1 - 2r \exp(-\frac{\beta}{8} k^{1-2\delta})$, the two-stage algorithm recovers $\{\mathbf{u}_i, \mathbf{v}_i\}$ from the sketch of size $m = 2R$ with running time $\mathcal{O}(rk^2 / \ln k)$.*
- 2) *When $r > 1$ and the $\{\mathbf{u}_i\}$ or $\{\mathbf{v}_i\}$ have overlapping supports, with probability at least $1 - \mathcal{O}(k^{-2})$, stage A of the algorithm followed by singular value decomposition of the recovered nonzero submatrix recovers $\{\mathbf{u}_i, \mathbf{v}_i\}$ from a sketch of size $m = 3rk^2$ with running time $\mathcal{O}((rk)^3)$.*

Remarks similar to those for the symmetric case (below Theorem 1) hold for the non-symmetric case as well.

3.1 Proof of Theorem 1

Part 1). In the setting of part 1), the eigenvectors $\{\mathbf{v}_i\}$ have disjoint supports with each \mathbf{v}_i being k -sparse. In this case, the nonzero entries of $\mathbf{X} = \sum_{i=1}^r \lambda_i \mathbf{v}_i \mathbf{v}_i^T$ form r disjoint submatrices, each of size $k \times k$. The result of Theorem 1 for this setting is proved via two lemmas, which give high probability bounds on the number of nonzero matrix entries recovered in stage A and the number of nonzero eigenvector entries recovered in stage B, respectively.

Lemma 3.1. *Consider the setting of part 1) of Theorem 1. Let \mathbf{A} be the fraction (out of $r\tilde{k}$) of nonzero entries in the upper triangular part of \mathbf{X} recovered in stage A. Then, with $\delta \in (0, 1)$ as defined in Theorem 1, there exists $\alpha^* = k^{-\delta} - o(k^{-\delta})$ such that for sufficiently large k ,*

$$\mathbb{P}\{\mathbf{A} \geq \alpha^*\} \geq 1 - 4 \exp\left(-\frac{dr}{17\delta^2} \frac{k^{2-\delta}}{\ln^2 k}\right). \quad (13)$$

Moreover, in the $k \times k$ nonzero submatrix corresponding to $\lambda_i \mathbf{v}_i \mathbf{v}_i^T$, let \mathbf{A}_i be the fraction (out of $\binom{k}{2}$) of above-diagonal entries recovered and let N_{D_i} be the number of diagonal entries recovered, for $i \in [r]$. Then there exists $\alpha_i^* = k^{-\delta} - o(k^{-\delta})$ for $i \in [r]$ such that for sufficiently large k ,

$$\mathbb{P} \{N_{D_i} \geq 1 \text{ and } \mathbf{A}_i \geq \alpha_i^*, \forall i \in [r]\} \geq 1 - 2r \exp\left(-\frac{1}{2}k^{1-\delta}\right). \quad (14)$$

The proof of the lemma, given in Section 5.2, first establishes that in the bipartite graph at the start of stage A (Fig. 1a), the degrees of the right nodes are each Binomial with mean $\delta \ln k$ and negatively associated. (Negative association is defined in Section 5.1). A Chernoff bound for negatively associated random variables is then used to obtain a high probability guarantee on the number of left nodes that are connected to singleton right nodes (and can hence be recovered).

The next lemma shows that the conditional probability of recovering all the nonzero entries in each eigenvector is close to 1, given the high probability event in (14).

Lemma 3.2. *Consider the setting of part 1) of Theorem 1 and let $N_{D_i}, \mathbf{A}_i, \alpha_i^*$ be as defined in Lemma 3.1. Let \mathbf{B}_i be the fraction (out of k) of nonzero entries of \mathbf{v}_i that are recovered by the end of stage B. Then, for all $N_{D_i} \geq 1, \mathbf{A}_i \geq \alpha_i^*$ and sufficiently large k we have:*

$$\mathbb{P} \{\mathbf{B}_i < 1 \mid N_{D_i}, \mathbf{A}_i\} < \exp\left(-\frac{1}{30}k^{1-\delta}\right), \quad i \in [r]. \quad (15)$$

The proof of the lemma is given in Section 5.3. Recall that on each subgraph $i \in [r]$ in stage B, the algorithm sequentially identifies and peels off left nodes connected to degree-1 right nodes. To successfully recover all the k nonzeros in the corresponding eigenvector \mathbf{v}_i , the residual graph needs to have at least one degree-1 right node at the end of each iteration $0 \leq t \leq (k-2)$. Conditioned on \mathbf{A}_i and the high-probability event in (14), we show that at the start of each iteration t , the number of degree-1 right nodes connected to each remaining left node is approximately Binomial with mean $\mathbf{A}_i t$ (See Lemma 5.7). This is then used to show that with high probability, there is at least one degree-1 right node in each iteration until all the k nonzeros are recovered.

Proof of part 1) of Theorem 1: From Lemmas 3.1 and 3.2, for sufficiently large k we have:

$$\begin{aligned} & \mathbb{P} \{\mathbf{B}_i = 1, \forall i \in [r]\} \\ & \geq \mathbb{E} \left[\mathbb{P} \{\mathbf{B}_i = 1, \forall i \in [r] \mid (N_{D_i}, \mathbf{A}_i)_{i \in [r]}\} \mathbb{1}\{N_{D_i} \geq 1 \text{ and } \mathbf{A}_i \geq \alpha_i^*, \forall i \in [r]\} \right] \\ & \stackrel{(i)}{\geq} \left(1 - r \exp\left(-\frac{1}{30}k^{1-\delta}\right)\right) \mathbb{P} \{N_{D_i} \geq 1 \text{ and } \mathbf{A}_i \geq \alpha_i^*, \forall i \in [r]\} \\ & \stackrel{(ii)}{\geq} \left(1 - r \exp\left(-\frac{1}{30}k^{1-\delta}\right)\right) \left(1 - 2r \exp\left(-\frac{1}{2}k^{1-\delta}\right)\right) \\ & > 1 - 2r \exp\left(-\frac{1}{2}k^{1-\delta}\right) - r \exp\left(-\frac{1}{30}k^{1-\delta}\right) > 1 - 2r \exp\left(-\frac{1}{30}k^{1-\delta}\right), \end{aligned} \quad (16)$$

where the inequality (i) is obtained from (15) along with a union bound. The inequality (ii) follows from (14). This completes the proof of part 1) of Theorem 1. \square

Part 2). When $\{\mathbf{v}_i\}$ have overlapping supports, recall from Section 2.3 that the algorithm recovers all the nonzero entries of \mathbf{X} , and then performs an eigendecomposition on the recovered nonzero submatrix. In this case, the first stage is equivalent to the compressed sensing recovery of the

vectorized matrix \mathbf{X} using the scheme of [1,2]. Theorem 4 in [1] shows that the compressed sensing scheme can recover a K -sparse vector with probability at least $1 - \mathcal{O}(1/K)$ with a sample complexity of $3K$ and running time $\mathcal{O}(K)$. This result directly yields the high probability guarantee in part 2) by noting that the number of nonzeros in the vectorized upper-triangular part of \mathbf{X} is bounded below by $\binom{k}{2} + k$ and above by $r\binom{k}{2} + k$.

3.2 Proof of Theorem 2

Part 1) Part 1) of the theorem is proved using the following two lemmas which characterize the high probability performance of stage A and stage B, respectively.

Lemma 3.3. *Consider the setting of part 1) of Theorem 2. Let \mathbf{A}_i denote the fraction of entries recovered in the $k \times \beta k$ nonzero submatrix corresponding to $\sigma_i \mathbf{u}_i \mathbf{v}_i^T$, for $i \in [r]$. Then, with $\delta \in (0, \frac{1}{2})$ as defined in Theorem 2, there exists $\alpha_i^* = k^{-\delta} - o(k^{-\delta})$ for $i \in [r]$ such that for sufficiently large k ,*

$$\mathbb{P}\{\mathbf{A}_i \geq \alpha_i^*, \forall i \in [r]\} \geq 1 - 2r \exp\left(-\frac{\beta}{4}k^{\frac{3}{2}-\delta}\right). \quad (17)$$

Lemma 3.4. *Consider the setting of part 1) of Theorem 2, and let \mathbf{A}_i, α_i^* be as defined in Lemma 3.3. Let \mathbf{B}_i^u and \mathbf{B}_i^v be the fraction of nonzeros in \mathbf{u}_i and \mathbf{v}_i , respectively, that are recovered in stage B. Then, for all $\mathbf{A}_i \geq \alpha_i^*$ and sufficiently large k , we have*

$$\mathbb{P}\{\mathbf{B}_i^u < 1 \text{ or } \mathbf{B}_i^v < 1 \mid \mathbf{A}_i\} \leq \exp\left(-\frac{\beta}{8}k^{1-2\delta}\right), \quad i \in [r]. \quad (18)$$

The proofs of Lemmas 3.3 and 3.4 are similar to those of Lemmas 3.1 and 3.2, respectively. We describe the main steps and highlight the key differences from the symmetric case in Sections 5.4 and 5.5.

Part 1) of Theorem 2 follows from Lemmas 3.3 and 3.4. Indeed, for sufficiently large k , we have:

$$\begin{aligned} & \mathbb{P}\{\mathbf{B}_i^u = 1 \text{ and } \mathbf{B}_i^v = 1, \forall i \in [r]\} \\ & \geq \mathbb{E}[\mathbb{P}\{\mathbf{B}_i^u = 1 \text{ and } \mathbf{B}_i^v = 1, \forall i \in [r] \mid \mathbf{A}_i, i \in [r]\} \mathbb{1}\{\mathbf{A}_i \geq \alpha_i^*, \forall i \in [r]\}] \\ & \stackrel{(i)}{\geq} \left(1 - r \exp\left(-\frac{\beta}{8}k^{1-2\delta}\right)\right) \mathbb{P}\{\mathbf{A}_i \geq \alpha_i^*, \forall i \in [r]\} \\ & \stackrel{(ii)}{\geq} \left(1 - r \exp\left(-\frac{\beta}{8}k^{1-2\delta}\right)\right) \left(1 - 2r \exp\left(-\frac{\beta}{4}k^{\frac{3}{2}-\delta}\right)\right) \\ & \geq 1 - r \exp\left(-\frac{\beta}{8}k^{1-2\delta}\right) - 2r \exp\left(-\frac{\beta}{4}k^{\frac{3}{2}-\delta}\right) \geq 1 - 2r \exp\left(-\frac{\beta}{8}k^{1-2\delta}\right). \end{aligned} \quad (19)$$

Here the inequality (i) is obtained using Lemma 3.4, and (ii) using Lemma 3.3. \square

Part 2). This proof is similar to the symmetric case (part 2) of Theorem 1). Indeed, applying [1, Theorem 4] guarantees that with probability $1 - \mathcal{O}(k^{-2})$, stage A of the algorithm recovers all the nonzero entries in the matrix. The nonzeros in the singular vectors are then obtained via a singular value decomposition on the recovered nonzero submatrix.

3.3 Computational cost of the recovery algorithm

We discuss the running time in the symmetric case, with the non-symmetric case being analogous.

Eigenvectors with disjoint supports. Consider the setting of part 1) of Theorem 1, where the supports of $\{\mathbf{v}_i\}$ are disjoint. Lemma 3.1 guarantees that for any $\delta \in (0, 1)$ and sufficiently large k , the fraction A of nonzero entries of \mathbf{X} recovered in stage A is at least $k^{-\delta}(1 - o(1))$ with high probability. We will analyze the complexity of the two stages assuming that $A = k^{-\delta}(1 - o(1))$. This is without loss of generality as one can terminate stage A of the algorithm (prematurely) once a fraction $k^{-\delta}(1 - o(1))$ of nonzero entries of \mathbf{X} have been recovered. From the proof of Lemma 3.1, this also means that the fraction of entries recovered in the nonzero submatrix corresponding to $\lambda_i \mathbf{v}_i \mathbf{v}_i^T$ is $A_i \sim k^{-\delta}$, for each $i \in [r]$. By Lemma 3.2, this is sufficient for recovering each \mathbf{v}_i with high probability.

Stage A: To begin, each of the R sketch bins requires $\mathcal{O}(1)$ numerical operations to be classified via a zero-ton test and a singleton test (specified in (12)). This requires a total of $\mathcal{O}(R) = \mathcal{O}(rk^2/\ln k)$ operations. In each peeling iteration, the contribution of a nonzero matrix entry is subtracted from the d bins that it is involved in and these bins are re-classified. Since d is a constant, each peeling iteration requires $\mathcal{O}(1)$ operations. By the termination assumption above, the number of iterations in stage A is $\mathcal{O}(rk^2A) = \mathcal{O}(rk^{2-\delta})$, corresponding to $\mathcal{O}(rk^{2-\delta})$ operations. Therefore, the total computational cost for stage A is $\mathcal{O}(rk^2/\ln k) + \mathcal{O}(rk^{2-\delta}) = \mathcal{O}(rk^2/\ln k)$.

Stage B: Recall that the graph at the start of stage B consists of r disjoint subgraphs, each with k left nodes representing the nonzero entries in the corresponding eigenvector and right nodes representing nonzero pairwise products recovered in stage A. Lemma 5.6 shows that with high probability, the degree of each left node in the i -th subgraph is $\mathcal{O}(A_i k)$. Since we assumed that $A_i \sim k^{-\delta}$, the degree of each left node is $\mathcal{O}(k^{1-\delta})$ with high probability. The algorithm peels off one left node at a time, and the cost of each peeling iteration is proportional to the number of edges peeled off during the iteration. Thus, to peel off all the k left nodes from the i -th subgraph, the computational cost is $\mathcal{O}(k^{2-\delta})$. Since there are r subgraphs, the total computational cost for stage B is $\mathcal{O}(rk^{2-\delta})$.

Finally, adding the costs for the two stages gives a total computational cost of $\mathcal{O}(rk^2/\ln k)$.

Eigenvectors with overlapping supports. In the setting of part 2) of Theorem 1, the algorithm recovers all the nonzero matrix entries in stage A. In this case, the number of nonzeros and the number of bins R are both $\mathcal{O}(rk^2)$. Therefore, the computational cost of stage A is $\mathcal{O}(rk^2)$. The nonzeros in the eigenvectors are then recovered by an eigendecomposition of the recovered nonzero submatrix. Since this submatrix has size at most $rk \times rk$, the computational cost of the eigendecomposition is $\mathcal{O}((rk)^3)$, which dominates the total cost of the algorithm.

3.4 Numerical results

We investigate the empirical performance of the scheme for both symmetric and non-symmetric matrices, with k -sparse signal vectors $\{\mathbf{u}_i, \mathbf{v}_i\}$ that have disjoint or overlapping supports. In the simulations, each signal vector \mathbf{u}_i or \mathbf{v}_i is obtained by first sampling its k nonzero entries from the mixture of Gaussians $\frac{1}{2}\mathbf{N}(-5, 1) + \frac{1}{2}\mathbf{N}(5, 1)$ and then normalizing so that the resulting vector has unit norm. When $\{\mathbf{u}_i\}$ and $\{\mathbf{v}_i\}$ have overlapping supports, we use the Gram–Schmidt process to ensure both sets of signal vectors are orthogonal. The number of ones in each column of the parity check matrix \mathbf{H} is chosen to be $d = 2$.

In Fig. 4, we declare exact recovery if: i) the locations of the nonzeros in the signal vectors are correctly recovered and the values of the nonzeros are recovered within an absolute deviation of 10^{-7} from the ground truth, and ii) the eigenvalues or singular values are also recovered within an

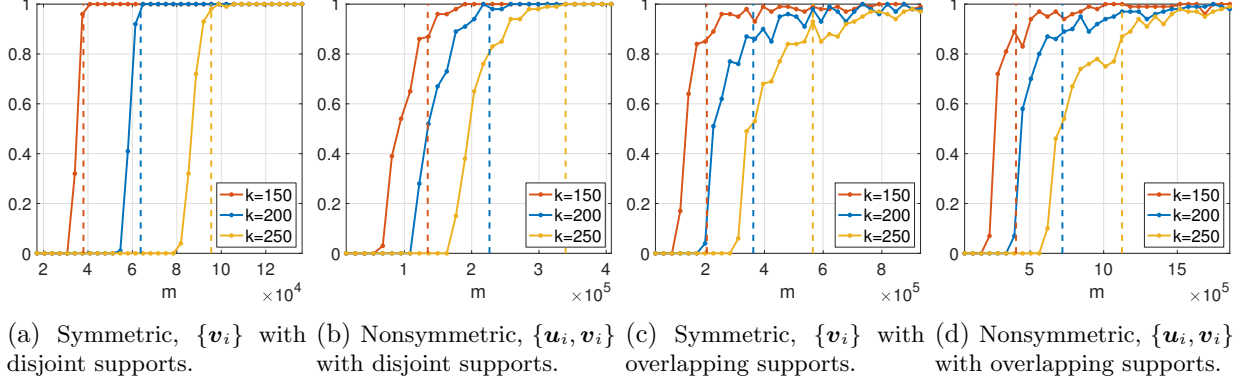


Figure 4: Probability of exact recovery (y -axis) versus sketch size m (x -axis), for different sparsity levels k . The matrices used in all cases have rank $r = 3$ and size $n \times n$ with $n = 10^4$. The dashed lines indicate the sketch sizes stated in Theorems 1 and 2; the dashed lines in (a) and (b) are determined using $\delta = \frac{5}{7}$ and $\delta = \frac{2}{5}$, respectively. Results are averaged over 100 trials.

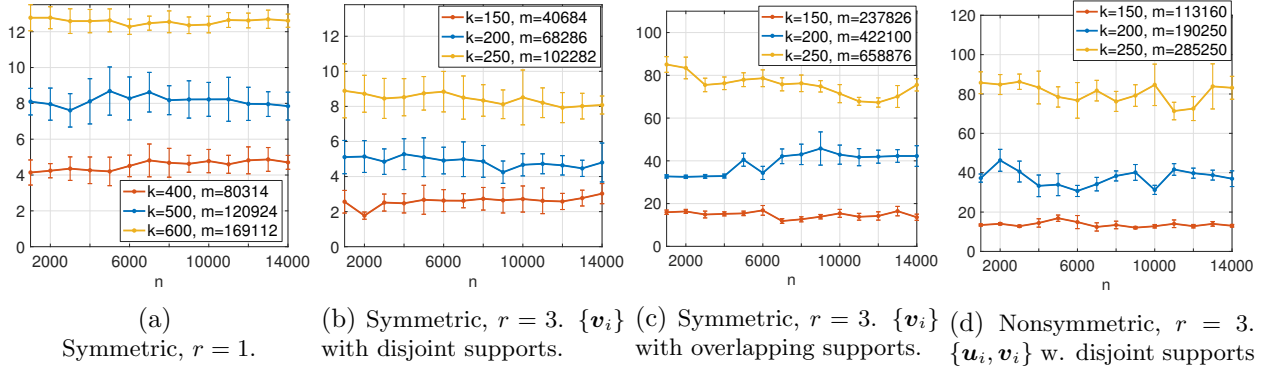


Figure 5: Running time (in secs) of the recovery algorithm versus ambient dimension n , for different sparsity levels k and sketch sizes m . Exact recovery is achieved in every trial. Results are averaged over 50 trials and error bars indicate one standard deviation.

absolute deviation of 10^{-7} from the ground truth. In each subfigure of Fig. 4, we plot the fraction of trials in which exact recovery is achieved versus the sketch size m , for different sparsity levels k . In Figs. 4a–4b, the dashed lines show the sketch sizes specified in part 1) of Theorems 1 or 2 for the values of δ indicated in the caption. The figures illustrate that for a fixed δ , the success probability at the sketch size corresponding to the dashed lines increases with k . In Figs. 4c–4d, the dashed lines indicate the sketch size specified in part 2) of the theorems. The empirical success probability at the dashed lines similarly increases with k .

Each subfigure in Fig. 5 plots the running time of the recovery algorithm (Matlab implementation) versus the ambient dimension n , for three different sparsity levels k and sketch sizes m . The plots confirm that the running time of the algorithm does not depend on n . The running times in different subfigures are not comparable because the experiments were executed at different times on a shared machine.

Fig. 6 compares our scheme with a conventional scheme which uses an i.i.d. Gaussian sketching operator and recovers the signal matrix \mathbf{X} (assumed to be positive semidefinite (PSD)) by solving

the convex program:

$$\hat{\mathbf{X}} \in \arg \min_{\mathbf{X} \succeq 0} \|\bar{\mathbf{X}}\|_* + \lambda \|\bar{\mathbf{X}}\|_1 \quad \text{subject to} \quad \mathcal{A}(\bar{\mathbf{X}}) = \mathcal{A}(\mathbf{X}), \quad (20)$$

where $\lambda \geq 0$. Here $\|\cdot\|_*$ and $\|\cdot\|_1$ denote the nuclear norm and ℓ_1 -norm, respectively. Each eigenvector of \mathbf{X} has k nonzero entries chosen independently from the Gaussian mixture distribution $\frac{1}{2}\mathbf{N}(-5, 1) + \frac{1}{2}\mathbf{N}(5, 1)$. We use $\lambda = 0.25$ in (20), following the choice of in [32, Fig. 7]. It was shown in [32, Thm. 3(c1)] that recovering \mathbf{X} via this convex program requires $m = \Omega(\min\{k^2, rn\})$ measurements, as opposed to $m = \mathcal{O}(rk^2)$ measurements required by our scheme. This indicates that our scheme requires smaller sample complexity in the very sparse regime (i.e., when $k = o(\sqrt{n})$), whereas the conventional scheme is more sample efficient when the signal vectors are relatively dense. This is reflected in Figs. 6a and 6b, where k is fixed in each plot: the sketch size m required for accurate recovery increases with n for the conventional scheme, while it remains largely constant for our scheme. Moreover, our algorithm exhibits a sharp transition in normalized error as m increases for any fixed n , whereas the conventional approach has a sharp transition only when n is relatively small (the less sparse regime).

The optimization program (20) is solved using CVX [41, 42] with the commercial solver MOSEK (version 10.0.25) [43], which runs faster than other solvers such as SDPT3 and SeDuMi. Alternatively, we tried solving the dual problem using TFOCS [44], which was developed in particular for sparse recovery applications, and discovered that this was slower than the CVX implementation.

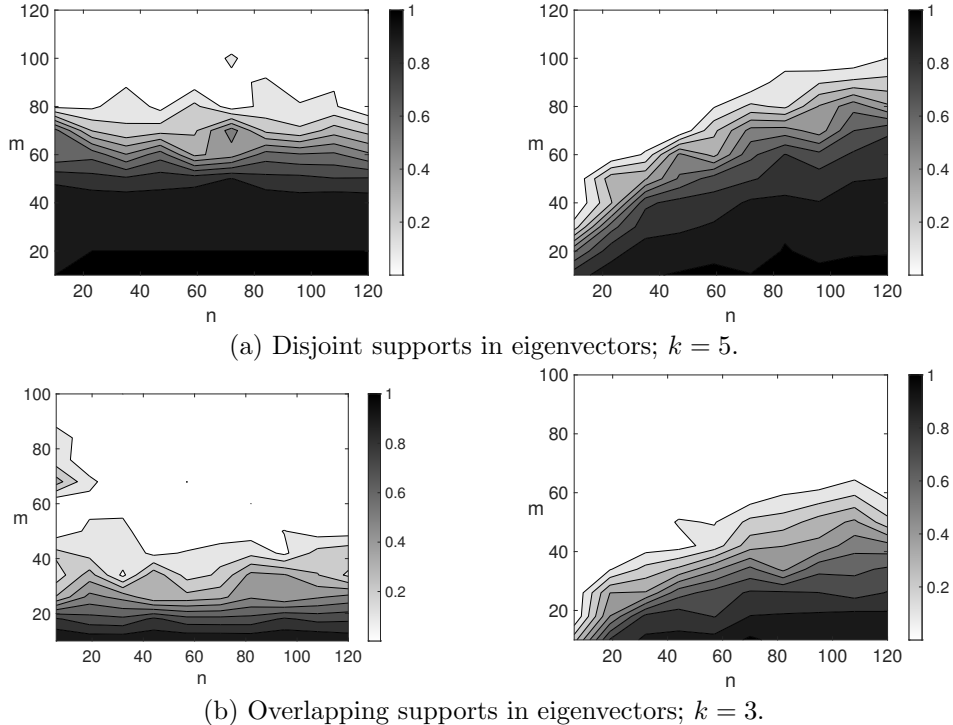
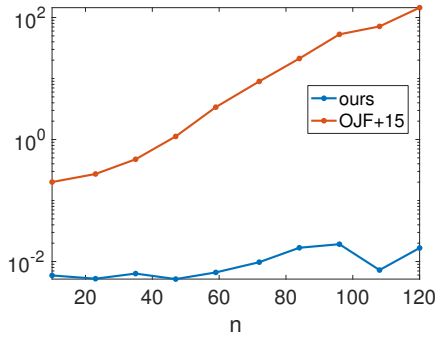
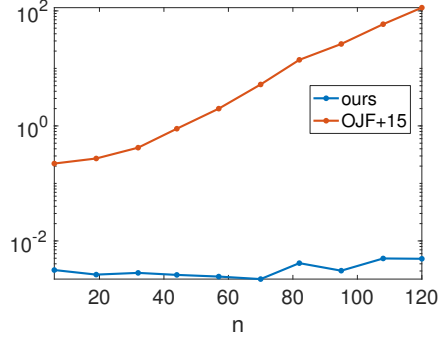


Figure 6: Normalized error $\|\hat{\mathbf{X}} - \mathbf{X}\|_F / \|\mathbf{X}\|_F$ of our scheme (left column), and the conventional scheme (right) using a Gaussian sketching operator and recovery via the convex program in (20). Each heatmap shows the normalized error across different ambient dimension n (x -axis) and number of measurements m (y -axis) for a fixed k . Results are averaged over 10 trials.



(a) Same setting as in Fig. 6a. Fix $k = 5, m = 100$ and vary n .



(b) Same setting as in Fig. 6b. Fix $k = 3, m = 84$ and vary n .

Figure 7: Running time of our scheme and the conventional scheme using a Gaussian sketching operator and recovery via the convex program in (20). Same setting as in Fig. 6. Each plot shows the running time against n , for a fixed k and m .

We also observe that the convex program converges faster with the PSD constraint in (20) than without, while our algorithm doesn't need this constraint.

Even though we use the most powerful packages, the convex program becomes prohibitively slow when the matrix size grows beyond 100×100 . For this reason, we restrict our experiments to small matrices up to 120×120 . The running time of the experiments in Fig. 6 is plotted in Fig. 7 for a specific m . We observe that our algorithm is 2 to 4 orders of magnitude faster than the convex optimization algorithm. Moreover, the running time of the convex program grows with n , while our iterative algorithm doesn't. (The small increase in our running time in Fig. 7 with n is an artefact since k is small here). Hence our scheme scales well to much larger n and k , as demonstrated by Fig. 5.

4 Recovery in the presence of noise

Consider the general model for the data matrix \mathbf{X} in (2):

$$\mathbf{X} = \mathbf{X}_0 + \mathbf{W}, \quad \text{where } \mathbf{X}_0 = \sum_{i=1}^r \lambda_i \mathbf{v}_i \mathbf{v}_i^T \text{ (symmetric) or } \mathbf{X}_0 = \sum_{i=1}^r \sigma_i \mathbf{u}_i \mathbf{v}_i^T \text{ (non-symmetric).} \quad (21)$$

The vectors \mathbf{v}_i and \mathbf{u}_i are k -sparse, for $i \in [r]$. In the non-symmetric case, the elements of the noise matrix \mathbf{W} are assumed to be independent and identically distributed with zero mean and variance σ^2 . We assume that σ^2 or at least a good upper bound on σ^2 is known. In the symmetric case, the same assumption holds for the upper triangular entries, with $W_{\ell,j} = W_{j,\ell}$ for $j < \ell \in [n]$.

4.1 Sketching scheme

We describe the scheme for symmetric matrices, with the non-symmetric case being analogous. We write $\mathbf{x}, \mathbf{x}_0, \mathbf{w}$ for the vectorized upper-triangular parts of the symmetric matrices $\mathbf{X}, \mathbf{X}_0, \mathbf{W}$, respectively. As before, we let $\tilde{n} = \binom{n}{2} + n$ and $\tilde{k} = \binom{k}{2} + k$. As in the noiseless setting (Section 2.1), the sketching matrix \mathbf{B} is formed by combining two matrices: a sparse parity check matrix

\mathbf{H} , and a matrix \mathbf{S} that helps classify each sketch bin as a zero-ton, singleton, or multi-ton. When there is noise, we cannot reliably identify zero-ton and singleton by simply taking \mathbf{S} to be the first two rows of an \tilde{n} -point DFT matrix as in (5). Therefore, following [1], we choose $\mathbf{S} \in \mathbb{R}^{P \times \tilde{n}}$ with

$$P = \mathcal{O}\left(\log\left(\frac{n}{k}\right)\right) \quad \text{and} \quad S_{\kappa,\ell} \stackrel{\text{iid}}{\sim} \mathbf{N}(0,1), \quad \kappa \in [P], \ell \in [\tilde{n}]. \quad (22)$$

The sparse parity check matrix $\mathbf{H} \in \{0,1\}^{R \times \tilde{n}}$ is chosen in the same way as in the noiseless setting: column-regular with $d \geq 2$ ones per column in uniformly random locations. The sketching matrix $\mathbf{B} \in \mathbb{R}^{PR \times \tilde{n}}$ is then formed as the column-wise Kronecker product of \mathbf{H} and \mathbf{S} , computed as illustrated in (7)–(8). The sketch $\mathbf{y} = \mathbf{B}\mathbf{x}$ has size $m = PR$.

We can view the sketch \mathbf{y} as comprising R bins, each with P entries. For $j \in [R]$, we let $\mathbf{y}_j := [y_{(Pj-P+1)}, \dots, y_{(Pj)}]^T \in \mathbb{R}^P$ be the j -th sketch bin. Similarly to (9) and (10), writing $\mathbf{B}_j \in \mathbb{R}^{P \times \tilde{n}}$ for the j -th set of P rows in \mathbf{B} , we have

$$\mathbf{y}_j = \mathbf{B}_j \mathbf{x} = \mathbf{S} \mathbf{x}_{0j}^* + \mathbf{S} \mathbf{w}_j^*, \quad j \in [R], \quad (23)$$

where the entries of $\mathbf{x}_{0j}^* \in \mathbb{R}^{\tilde{n}}$ and $\mathbf{w}_j^* \in \mathbb{R}^{\tilde{n}}$ are

$$(x_{0j}^*)_\ell = \begin{cases} x_{0\ell} & \ell \in \mathcal{N}(j) \\ 0 & \ell \notin \mathcal{N}(j) \end{cases}, \quad (w_j^*)_\ell = \begin{cases} w_\ell & \ell \in \mathcal{N}(j) \\ 0 & \ell \notin \mathcal{N}(j) \end{cases} \quad \text{for } \ell \in [\tilde{n}]. \quad (24)$$

As in (10), $\mathcal{N}(j) = \{\ell \in [\tilde{n}] : H_{j,\ell} = 1\}$ contains the locations of the ones in the j -th row of \mathbf{H} . The vectors \mathbf{x}_{0j}^* and \mathbf{w}_j^* store the signal and noise entries that contribute to the j -th bin. The j -th bin \mathbf{y}_j is the sum of these entries weighted by their respective columns in \mathbf{S} .

4.2 Recovery algorithm

We first consider symmetric rank- r matrices where $\{\mathbf{v}_1, \dots, \mathbf{v}_r\}$ have disjoint supports. Fix $\delta \in (0,1)$, let $R = dr\tilde{k}/(\delta \ln k)$, and recall that the sketch size is $m = PR$.

4.2.1 Accumulated noise variance in each bin

The recovery of \mathbf{x} crucially depends on the variance of the noise vector $\mathbf{S}\mathbf{w}_j^*$ in each sketch bin \mathbf{y}_j (see (23)). Since \mathbf{H} has d ones per column, each entry of \mathbf{x} contributes to d bins, chosen uniformly at random from the R bins in the sketch. Thus we have $|\mathcal{N}(j)| \sim \text{Bin}(\tilde{n}, \frac{d}{R})$. Noting that $\mathbb{E}\{|\mathcal{N}(j)|\} = \frac{\tilde{n}d}{R} = \left(\binom{n}{2} + n\right) \frac{\delta \ln k}{rk}$, we apply the tail bound in Lemma 5.1 to obtain

$$\mathbb{P}\left\{|\mathcal{N}(j)| \leq \frac{\delta n^2 \ln k}{4 rk^2}\right\} \leq \exp\left(-\frac{\delta n^2 \ln k}{7 rk^2}\right). \quad (25)$$

Writing $\tilde{\mathbf{w}}_j^* := \mathbf{S}\mathbf{w}_j^*$ for the noise vector in (23), the entries in $\tilde{\mathbf{w}}_j^*$ are:

$$(\tilde{w}_j^*)_\kappa = \sum_{\ell \in \mathcal{N}(j)} S_{\kappa,\ell} w_\ell, \quad \text{for } \kappa \in [P]. \quad (26)$$

Recalling that w_ℓ is zero-mean with variance σ^2 and i.i.d. across ℓ , conditioned on \mathbf{S} and $\mathcal{N}(j)$, the vector $\tilde{\mathbf{w}}_j^*$ is zero-mean with covariance matrix $\Sigma \in \mathbb{R}^{P \times P}$, where

$$\Sigma_{\kappa,\kappa} = \sigma^2 \sum_{\ell \in \mathcal{N}(j)} S_{\kappa,\ell}^2, \quad \Sigma_{\kappa,\iota} = \sigma^2 \sum_{\ell \in \mathcal{N}(j)} S_{\kappa,\ell} S_{\iota,\ell} \quad \text{for } \kappa, \iota \in [P] \text{ and } \kappa \neq \iota. \quad (27)$$

Since \mathbf{S} has independent standard Gaussian entries, $\mathbb{E}[S_{\kappa,\ell}^2] = 1$ and $\mathbb{E}[S_{\kappa,\ell}S_{\iota,\ell}] = 0$. Moreover, (25) implies that $|\mathcal{N}(j)| \rightarrow \infty$ almost surely as $n \rightarrow \infty$. Therefore, by the weak law of large numbers, $\frac{\sum_{\kappa,\kappa}}{|\mathcal{N}(j)|} \rightarrow \sigma^2$ and $\frac{\sum_{\kappa,\iota}}{|\mathcal{N}(j)|} \rightarrow 0$ as $n \rightarrow \infty$. It follows that the distribution of the scaled accumulated noise vector $\frac{\tilde{\mathbf{w}}_j^*}{\sqrt{|\mathcal{N}(j)|}}$ converges to the Gaussian $\mathbf{N}(\mathbf{0}, \sigma^2 \mathbf{I}_P)$ as $n \rightarrow \infty$. We will use this limiting distribution to devise zero-ton and singleton tests in stage A of the algorithm.

4.2.2 Stage A of the algorithm

Zero-ton test. When \mathbf{y}_j is a zero-ton, i.e., when $\text{supp}(\mathbf{x}_0) \cap \mathcal{N}(j) = \emptyset$, from (23) and (24) we have

$$\mathbf{y}_j = \mathbf{S}\mathbf{w}_j^* = \tilde{\mathbf{w}}_j^*, \quad \text{with } \frac{\tilde{\mathbf{w}}_j^*}{\sqrt{|\mathcal{N}(j)|}} \text{ approximately } \sim \mathbf{N}(\mathbf{0}, \sigma^2 \mathbf{I}_P). \quad (28)$$

Based on this, a given bin \mathbf{y}_j is declared a zero-ton if

$$\frac{1}{P|\mathcal{N}(j)|} \|\mathbf{y}_j\|^2 \leq \gamma_0 \sigma^2, \quad (29)$$

for a suitably chosen constant γ_0 . Empirically, 99.7% of the samples of a Gaussian distribution lie within 3 standard deviations of the mean, so we set $\gamma_0 \geq 3$. In our experiments, $\gamma_0 = 5$ gives reasonable performance.

Singleton test. When \mathbf{y}_j is a singleton with $\text{supp}(\mathbf{x}_0) \cap \mathcal{N}(j) = \ell$, it takes the form

$$\mathbf{y}_j = x_{0\ell} \mathbf{s}_\ell + \tilde{\mathbf{w}}_j^*, \quad (30)$$

where \mathbf{s}_ℓ is the ℓ -th column of \mathbf{S} . Given any bin \mathbf{y}_j , assuming it is a singleton of the form (30), the algorithm first estimates the index ℓ and the value $x_{0\ell}$ as follows:

$$\hat{\ell} = \arg \min_{\ell \in \mathcal{N}(j)} \|\mathbf{y}_j - \hat{x}_{0\ell} \mathbf{s}_\ell\|^2, \quad \text{where } \hat{x}_{0\ell} = \frac{\mathbf{s}_\ell^T \mathbf{y}_j}{\|\mathbf{s}_\ell\|^2}. \quad (31)$$

The bin j is declared a singleton if

$$\frac{1}{P|\mathcal{N}(j)|} \|\mathbf{y}_j - \hat{x}_{0\hat{\ell}} \mathbf{s}_{\hat{\ell}}\|^2 \leq \gamma_1 \sigma^2, \quad (32)$$

for some constant $\gamma_1 \leq \gamma_0$. The estimated index-value pair $(\hat{\ell}, \hat{x}_{0\hat{\ell}})$ in (31) is the maximum-likelihood estimate of $(\ell, x_{0\ell})$ corresponding to the singleton bin in (30), given the limiting distribution of the noise $\frac{\tilde{\mathbf{w}}_j^*}{\sqrt{|\mathcal{N}(j)|}}$ is $\mathbf{N}(\mathbf{0}, \sigma^2 \mathbf{I}_P)$. We note that $(\hat{\ell}, \hat{x}_{0\hat{\ell}})$ will be an accurate estimate of the true index-value pair $(\ell, x_{0\ell})$ only when the accumulated noise level $\sqrt{|\mathcal{N}(j)|}\sigma$ (i.e., the standard deviation of $\tilde{\mathbf{w}}_j^*$) is much smaller than the signal magnitude $|x_{0\ell}|$.

The algorithm declares \mathbf{y}_j a multiton if it fails both zero-ton and singleton tests.

At $t = 0$, the algorithm identifies the initial set of zero-ton and singleton among the R bins using the tests above. Let $\mathcal{S}(t)$ denote the set of singletons at time t . Then at each $t \geq 1$, the algorithm picks a singleton uniformly at random from $\mathcal{S}(t-1)$, and recovers the nonzero entry of \mathbf{x}_0 underlying the singleton using the index-value pair $(\hat{\ell}, \hat{x}_{0\hat{\ell}})$ in (31). The algorithm then peels

off the contribution of the $\hat{\ell}$ -th entry of \mathbf{x}_0 from each of the d bins it is involved in, re-categorizes these bins, and updates the set of singletons to include any new singletons created by the peeling of the $\hat{\ell}$ -th entry. The updated set of singletons is $\mathcal{S}(t)$. Stage A continues until singletons run out, i.e., when $\mathcal{S}(t) = \emptyset$. This algorithm is similar to Algorithm 1 with additional input \mathcal{S} , γ_0 , γ_1 and σ^2 , and different zero-ton and singleton tests. We omit the pseudocode for brevity. If the supports of $\{\mathbf{v}_1, \dots, \mathbf{v}_r\}$ are known to be disjoint, we proceed to stage B, described in the next subsection.

When the supports of the r eigenvectors have overlaps, we take a large enough sketch (with $R = \mathcal{O}(rk^2)$) to identify all the nonzero entries in \mathbf{X}_0 in stage A, and then perform an eigendecomposition on the recovered submatrix of nonzero entries to obtain the nonzero entries of $\{\mathbf{v}_1, \dots, \mathbf{v}_r\}$.

Picking the threshold parameters γ_0, γ_1 : Decreasing the value of γ_0 makes the zero-ton test in (29) more stringent. As γ_0 becomes smaller, zero-tones are more likely to be mistaken as singletons with small signal values. This kind of error results in some zero entries of \mathbf{X}_0 being mistakenly recovered as small nonzeros. Since our recovery algorithm crucially relies on the sparsity of \mathbf{X}_0 to maintain its low complexity, empirically we find that such errors greatly increase the algorithm's running time. Moreover, in the case where $\{\mathbf{v}_i\}$ have disjoint supports, such errors can lead to stability issues in stage B when peeling steps involve taking ratios between small signal values. For these reasons, we set $\gamma_0 = 5$ in our numerical simulations. We set a more stringent threshold for the singleton test by choosing $\gamma_1 \leq \gamma_0$ to prevent multitons from being mistaken as singletons.

4.2.3 Stage B of the algorithm

In the stage B graph (Fig. 2a or Fig. 3a), the right nodes are the nonzero matrix entries (i.e., pairwise products) recovered in stage A. The values of these recovered entries are no longer exact in the noisy setting. Hence, a left node connected to multiple degree-1 right nodes will receive different suggested values from these right nodes. Therefore, instead of peeling off edges like in Section 2.2.2, we use a message passing algorithm on the stage B graph. In each iteration, all the left nodes with known values send these values to their neighboring right nodes. Recall that each right node in the stage B graph has two edges, and corresponds to the product of the two left nodes it is connected to. The message a right node sends along each edge is the ratio of its pairwise product with the incoming message along the other edge. Each left node then updates its value by taking the average of all messages it receives. This averaging operation makes the algorithm more robust to noise.

4.3 Sample complexity and computational cost

Disjoint supports We have $R = \mathcal{O}(rk^2/\ln k)$ bins and $P = \mathcal{O}(\log(n/k))$ components in each bin, therefore the sample complexity is $RP = \mathcal{O}(rk^2 \log(n/k)/\ln k)$, which is higher than the noiseless case by a factor of $P = \mathcal{O}(\log(n/k))$.

The computational cost of the recovery algorithm is $\mathcal{O}(n^2 \log(n/k))$, significantly higher than the $\mathcal{O}(rk^2/\ln k)$ in the noiseless setting. The increase in complexity is due to the singleton test in (31)–(32), which requires finding a minimum over the $|\mathcal{N}(j)|$ left nodes that connect to bin \mathbf{y}_j , for each $j \in [R]$. From (25) and a similar upper tail bound, we know that with high probability $|\mathcal{N}(j)|$ is of the order $n^2 \ln k/(rk^2)$. Therefore, the total computational cost of the singleton test for the R bins is $R|\mathcal{N}(j)|P = \mathcal{O}(n^2 \log(n/k))$, which dominates the cost of stage A. When the noise level is small (so that in stage A, zero matrix entries are not mistakenly recovered as nonzeros), stage

B has the same $\mathcal{O}(rk^{2-\delta})$ complexity as in the noiseless case. Thus the computational cost of the algorithm is dominated by stage A.

General case The sample complexity is $\mathcal{O}(rk^2 \log(n/k))$, again higher than the noiseless setting by a factor of $P = \mathcal{O}(\log(n/k))$. The computational cost of recovering all the nonzero entries of the signal matrix is $\mathcal{O}(n^2 \log(n/k))$ and that of the eigendecomposition of the recovered nonzero submatrix is $\mathcal{O}((rk)^3)$. Thus, the total cost of the algorithm is $\mathcal{O}(\max\{n^2 \log(n/k), (rk)^3\})$.

In the noisy setting, the nonzero matrix entries recovered in stage A will not be exact, which makes it hard to analyze the subsequent step (either stage B or eigendecomposition) and obtain a rigorous performance guarantee. This can be addressed by making suitable assumptions on the signal alphabet. The analysis is conceptually similar to the noiseless setting but with additional technical challenges, so it is omitted. In the following subsection, we demonstrate the performance of the scheme in the noisy case via numerical simulations.

4.4 Numerical results

We apply the robust sketching scheme and recovery algorithm to symmetric matrices $\mathbf{X} = \mathbf{X}_0 + \mathbf{W}$, with $\mathbf{X}_0 = \sum_{i=1}^r \mathbf{v}_i \mathbf{v}_i^T$ and \mathbf{W} a random symmetric noise matrix. Here, we have dropped the $\tilde{\cdot}$ notation for simplicity to let $\mathbf{v}_1, \mathbf{v}_2, \dots, \mathbf{v}_r$ denote the unnormalized eigenvectors. Throughout this section, the column weight of the parity check matrix \mathbf{H} is chosen to be $d = 2$.

Each \mathbf{v}_i is k -sparse with its nonzero entries drawn uniformly at random from a discrete alphabet $\{\pm 10, \pm 20, \dots, \pm 50\}$. When the supports of $\{\mathbf{v}_i\}$ overlap, we adjust in each \mathbf{v}_i a small number of nonzero entries to ensure orthogonality among the $\{\mathbf{v}_i\}$. The resulting eigenvalues of \mathbf{X}_0 are $\lambda_i = \|\mathbf{v}_i\|^2$ for $i \in [r]$. We measure the signal strength by the expected average eigenvalue $\lambda := \mathbb{E}[\frac{1}{r} \sum_{i=1}^r \lambda_i]$. The entries in the noise matrix \mathbf{W} are drawn i.i.d. up to symmetry from $\mathbf{N}(0, \sigma^2)$. Let $\lambda_{W,1} \geq \lambda_{W,2} \geq \dots \geq \lambda_{W,n}$ denote the eigenvalues of \mathbf{W} . From Wigner's semicircle law [45], we have that $\max_{i \in [r]} \frac{\lambda_{W,i}}{\sqrt{n}}$ concentrates around 2σ and that $\lim_{n \rightarrow \infty} \mathbb{E}[\frac{1}{n^2} \sum_{i=1}^n \lambda_{W,i}^2] = \sigma^2$. Thus, to ensure the right scaling in our signal to noise ratio (SNR), we define our SNR to be $\lambda/(\sqrt{n}\sigma)$.

Let $\hat{\mathbf{v}}_1, \hat{\mathbf{v}}_2, \dots, \hat{\mathbf{v}}_r$ denote the unnormalized eigenvectors recovered by the algorithm, and $\hat{\mathbf{X}}_0$ the estimated signal matrix computed using $\{\hat{\mathbf{v}}_i\}$. Fig. 8 shows the normalized squared error (NSE) of the recovered matrix (defined as $\|\hat{\mathbf{X}}_0 - \mathbf{X}_0\|_F^2 / \|\mathbf{X}_0\|_F^2$) and the average NSE of the recovered eigenvectors (defined as $\frac{1}{r} \sum_{i=1}^r \|\hat{\mathbf{v}}_i - \mathbf{v}_i\|_2^2 / \|\mathbf{v}_i\|_2^2$) against the sketch size m , for different SNR values. The three columns in Fig. 8 correspond to three different settings, as indicated by the captions. In each column, the top subfigure plots the matrix NSE and the bottom subfigure plots the eigenvector NSE.

In each subfigure, the solid lines correspond to the proposed algorithm with message passing decoding in stage B. The dotted lines trailing along the solid lines correspond to the algorithm with peeling decoding in stage B. As we can see, message passing consistently outperforms peeling decoding, offering slightly better noise robustness. Moreover, the horizontal dashed lines indicate the NSE of the baseline method without sketching – this directly computes the eigendecomposition of the matrix \mathbf{X} and estimates the signals using the top r eigenvectors. (The sample complexity of the baseline method is the number of distinct entries in \mathbf{X} , i.e., $\tilde{n} = \binom{n}{2} + n$.) Our NSEs approach the baseline NSEs as m increases, especially in the overlapping support case (Fig. 8c). For accurate recovery, that is, in the settings corresponding to the first data points after the transition in the plots, the required sketch size m is at least an order of magnitude smaller than \tilde{n} ; the running time of the recovery algorithm is also noticeably smaller than the baseline method.

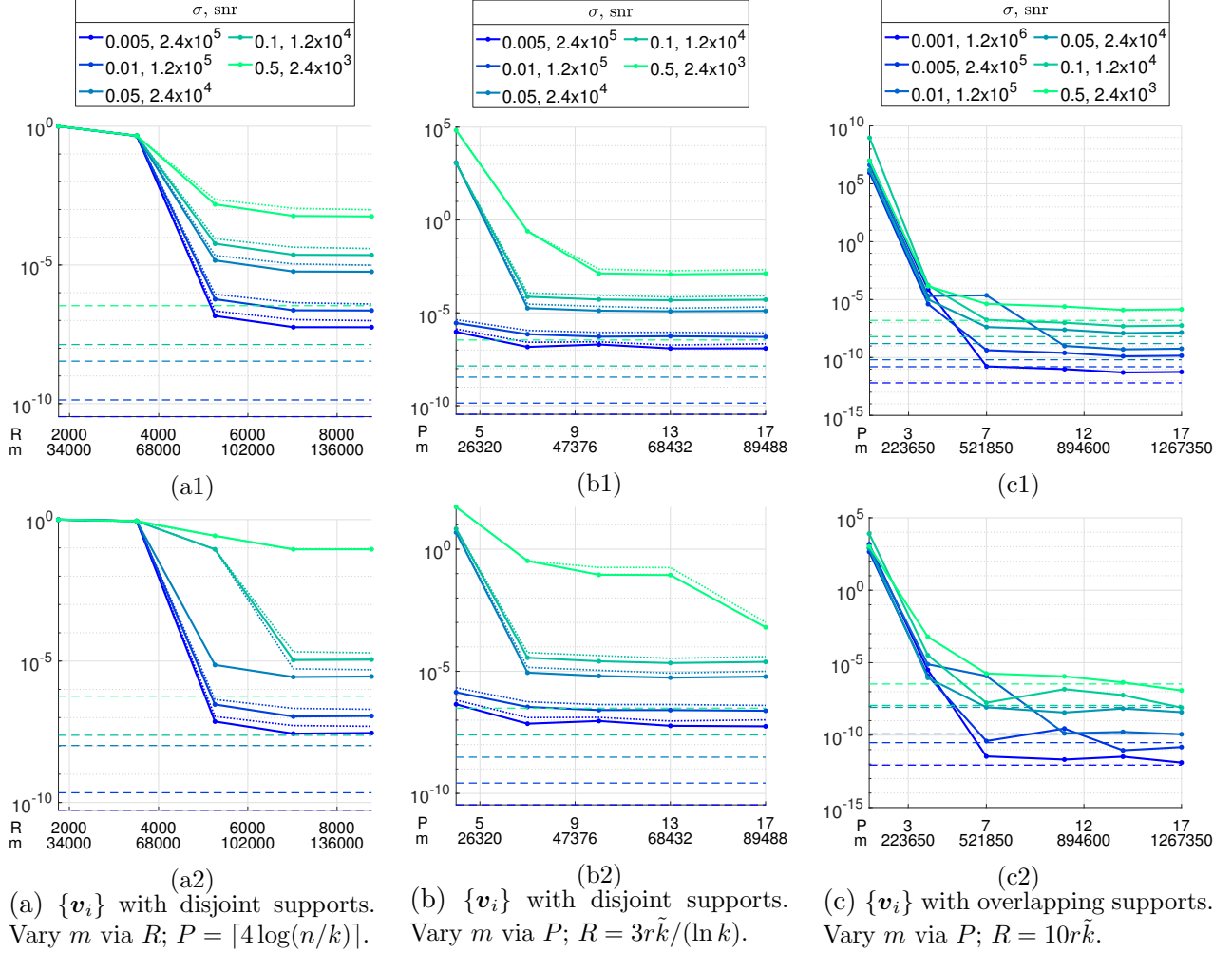


Figure 8: Normalized squared error of the matrix $\|\hat{\mathbf{X}}_0 - \mathbf{X}_0\|_F^2 / \|\mathbf{X}_0\|_F^2$ (top row) and average normalized square error of the eigenvectors $\frac{1}{r} \sum_{i=1}^r \|\hat{\mathbf{v}}_i - \mathbf{v}_i\|_2^2 / \|\mathbf{v}_i\|_2^2$ (bottom row) plotted against the sketch size m , for different SNRs $\lambda/(\sqrt{n}\sigma)$. Solid lines: proposed algorithm with message passing in stage B. Dotted lines: proposed algorithm with peeling decoding in stage B. Dashed lines: direct eigendecomposition of the noisy matrix and retain the contribution of the top r eigenvectors. In all cases, $n = 4000$, $k = 70$ and $r = 3$. The parameters in the zero-ton and singleton tests are $\gamma_0 = 5$ and $\gamma_1 = 2.5$ in (a)–(b) and $\gamma_1 = 3.5$ in (c). Results are averaged over 15 trials.

Recall that the sketch size is $m = RP$, where R is the number of bins and P is the number of components in each bin. In Fig. 8a, the sketch size is varied via R , with P held constant. As R increases, more nonzero matrix entries are recovered in the first stage of the algorithm. This increases the number of right nodes in the graph for stage B, allowing more nonzero eigenvector entries to be recovered which leads to smaller NSE. In Figs. 8b and 8c, the sketch size is varied via P , with the number of bins R held constant. The value of P is varied as $\lceil c \log(n/k) \rceil$ for $c \in [0.1, 4.1]$. The accuracy of the recovery improves as P increases due to more reliable zero-ton and singleton detection. In all subfigures, we observe that the NSEs decrease with the SNR as expected.

4.4.1 Comparison with alternative sketching schemes

We compare our scheme to two other existing methods. The first one uses an i.i.d. Gaussian sketching operator \mathcal{A} and a convex program similar to (20) for recovery, with an inequality constraint to account for the noise. In particular, to recover a PSD matrix \mathbf{X}_0 from the sketch $\mathcal{A}(\mathbf{X})$ where $\mathbf{X} = \mathbf{X}_0 + \mathbf{W}$, we solve the following optimization problem:

$$\hat{\mathbf{X}}_0 \in \arg \min_{\bar{\mathbf{X}} \succeq 0} \|\bar{\mathbf{X}}\|_* + \lambda \|\bar{\mathbf{X}}\|_1 \quad \text{subject to} \quad \|\mathcal{A}(\bar{\mathbf{X}}) - \mathcal{A}(\mathbf{X})\|_2 \leq \varepsilon_{n,m}, \quad (33)$$

where $\varepsilon_{n,m}$ is an upper bound on the ℓ_2 -norm of the noise vector $\mathbf{z} := \mathcal{A}(\mathbf{W})$. Recalling that $W_{ij} \stackrel{\text{iid}}{\sim} \mathbf{N}(0, \sigma^2)$ for $i \leq j$, we can deduce that $\mathbb{E}[\|\mathbf{z}\|_2^2] = mn^2\sigma^2$. Thus we set $\varepsilon_{n,m}^2 = 1.2mn^2\sigma^2$ in our experiments. Like in the noiseless case in Section 3.4 (Fig. 6), we use $\lambda = 0.25$, and solve (33) using CVX which calls the solver MOSEK.

In Fig. 9, we use rank-2 sparse PSD matrices $\mathbf{X}_0 = \sum_{i=1}^2 \mathbf{v}_i \mathbf{v}_i^T$. The nonzero entries of each \mathbf{v}_i are independently drawn from a mixture of Gaussians $\frac{1}{2}\mathbf{N}(-5, 1) + \frac{1}{2}\mathbf{N}(5, 1)$. The noise standard deviation is $\sigma = 0.1$ and the SNR is calculated as $\lambda/(\sqrt{n}\sigma)$ as before. For a fixed sparsity level $k = 3$, the heatmaps indicate the normalized error across different values of ambient dimension n

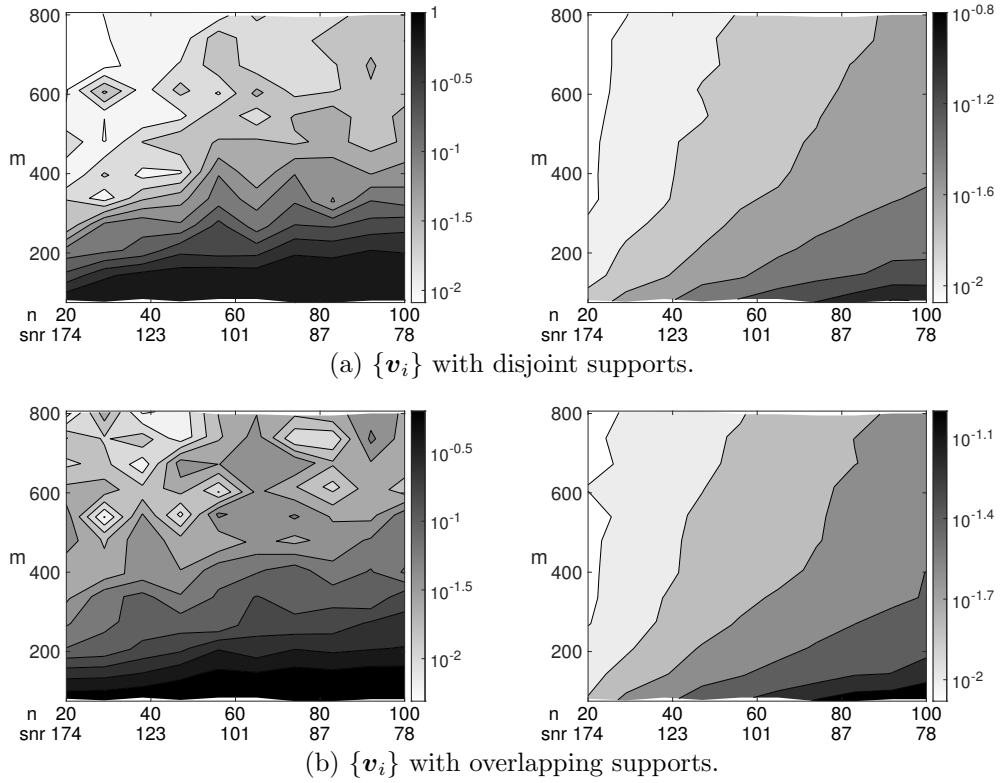


Figure 9: Normalized error $\|\hat{\mathbf{X}}_0 - \mathbf{X}_0\|_F / \|\mathbf{X}_0\|_F$ on \log_{10} scale. Left column: our scheme. Right column: conventional scheme using a Gaussian sketching operator and recovery via the convex program in (33). Each heatmap shows the normalized error across different values of ambient dimension n (x -axis) and number of measurements m (y -axis). The matrices \mathbf{X}_0 are rank-2 PSD matrices, with fixed sparsity level $k = 3$. The noise standard deviation is $\sigma = 0.1$ and SNR is $\lambda/(\sqrt{n}\sigma)$. $P = \lceil 4.5 \log(n/k) \rceil$, $\gamma_0 = 5$ and $\gamma_1 = 2.5$. Results are averaged over 30 trials.

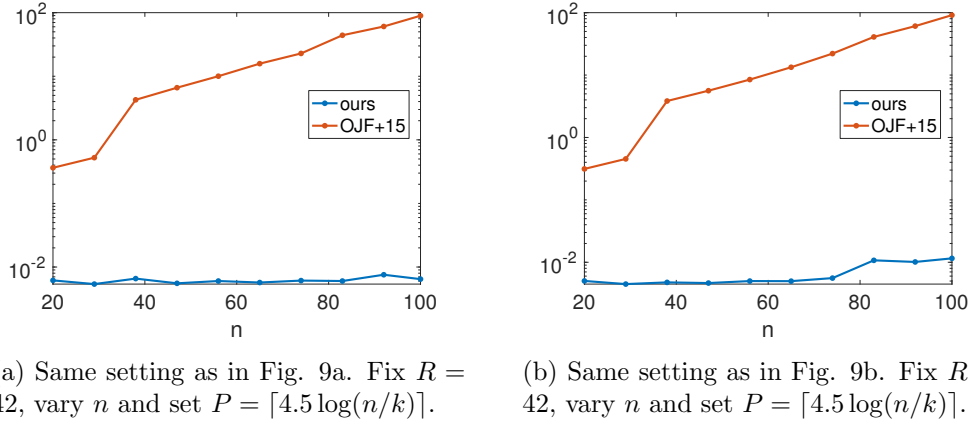


Figure 10: Running time of our scheme and the conventional scheme using Gaussian sketching operator and recovery via the convex program (33). Same setting as in Fig. 9. Each plot shows the running time against n , for fixed $k = 3$ and $R = 42$.

and sketch size m . We vary m via R , fixing P as $\lceil 4.5 \log(n/k) \rceil$ for each n value. Our experiments are restricted to small matrices, as the CVX solver for the convex program (33) is infeasibly slow for matrices bigger than 100×100 .

The left column of Fig. 9 corresponds to our scheme and the right to the optimization approach. We observe a similar trade-off as in the noiseless case (Fig. 6): the conventional scheme is more sample efficient in the relatively dense regime, but is outperformed by our scheme in the sparse regime given a sufficient number of measurements. Specifically, the normalized error in the top right region of the heatmaps is smaller under our scheme. It is worth noting that the contours in the heatmaps are significantly flatter under our scheme, indicating better scalability. The shallow gradient of the contours under our scheme is due to the $\log(n/k)$ factor in our sample complexity $m = \mathcal{O}(rk^2 \log(n/k))$.

Moreover, similar to the noiseless case, Fig. 10 shows that the running time of our algorithm grows much more slowly than the convex optimization method, and is several orders of magnitude faster across different n values.

The second scheme that we compare with is the nested scheme proposed in [35], [33, Sec. 3.3] for sketching PSD matrices. The sketching operator takes the form $\mathcal{A} : \mathbf{X} \rightarrow [\langle \mathbf{a}_i \mathbf{a}_i^T, \mathbf{X} \rangle]_{i=1}^m$ where $\mathbf{a}_i = \Psi^T \mathbf{e}_i \in \mathbb{R}^n$, with $\Psi \in \mathbb{R}^{L \times n}$ populated with entries $\stackrel{\text{iid}}{\sim} \mathcal{N}(0, 1/L)$, and $\mathbf{e}_1, \dots, \mathbf{e}_m \in \mathbb{R}^L \stackrel{\text{iid}}{\sim} \mathcal{N}(\mathbf{0}, \mathbf{I}_{L \times L})$. That is, each measurement takes the form

$$y_i = \langle \mathbf{a}_i \mathbf{a}_i^T, \mathbf{X} \rangle = \mathbf{a}_i^T \mathbf{X} \mathbf{a}_i = \mathbf{e}_i^T \Psi \mathbf{X} \Psi^T \mathbf{e}_i = \langle \mathbf{e}_i \mathbf{e}_i^T, \Psi \mathbf{X} \Psi^T \rangle =: \mathcal{E}(\Psi \mathbf{X} \Psi^T), \quad i \in [m]. \quad (34)$$

Note that \mathcal{A} has a nested structure, consisting of a linear operator \mathcal{E} and a matrix Ψ . With appropriately chosen L and m , \mathcal{E} forms a restricted isometry for low-rank matrices, and Ψ forms a restricted isometry for sparse matrices. This structure enables the following two-stage algorithm

to estimate \mathbf{X}_0 [33, 35]:

$$\text{Low-rank estimation stage: } \hat{\mathbf{B}} \in \arg \min_{\mathbf{B} \succeq 0} \text{trace}(\mathbf{B}) \quad \text{subject to} \quad \sum_{i=1}^m (e_i^T \mathbf{B} e_i - y_i)^2 \leq \varepsilon_{n,m}^2. \quad (35)$$

$$\text{Sparse estimation stage: } \hat{\mathbf{X}}_0 \in \arg \min_{\mathbf{X}} \|\bar{\mathbf{X}}\|_1 \quad \text{subject to} \quad \|\Psi \bar{\mathbf{X}} \Psi^T - \hat{\mathbf{B}}\|_F \leq \frac{C\varepsilon_{n,m}}{\sqrt{m}}. \quad (36)$$

Here C is a suitable constant, and $\varepsilon_{n,m}$ is an upper bound on the ℓ_2 -norm of the noise vector \mathbf{z} , whose entries take the form $z_i = e_i^T \Psi \mathbf{W} \Psi^T e_i$ for $i \in [m]$. Omitting the details, we use $\varepsilon_{n,m} = 1.5\sqrt{\mathbb{E}[\|\mathbf{z}\|_2^2]} = 1.5\sigma\sqrt{mn(n+2)(1+2/L)}$ in our experiments.

Fig. 11 compares the performance of our scheme with the nested sketching scheme for two different choices for the nonzero entries of the eigenvectors. These entries are drawn independently from either: (i) the Gaussian mixture distribution $\frac{1}{2}\mathbf{N}(-5, 1) + \frac{1}{2}\mathbf{N}(5, 1)$ or (ii) the uniform distribution over the discrete alphabet $\{\pm 10, \pm 20, \dots, \pm 50\}$. The matrix \mathbf{X}_0 is 100×100 rank-2 PSD, with eigenvectors having disjoint supports. We observe that our scheme consistently outperforms the nested scheme of [33, 35] in the sparse setting (Figs. 11a–11b). In the denser setting (Figs.

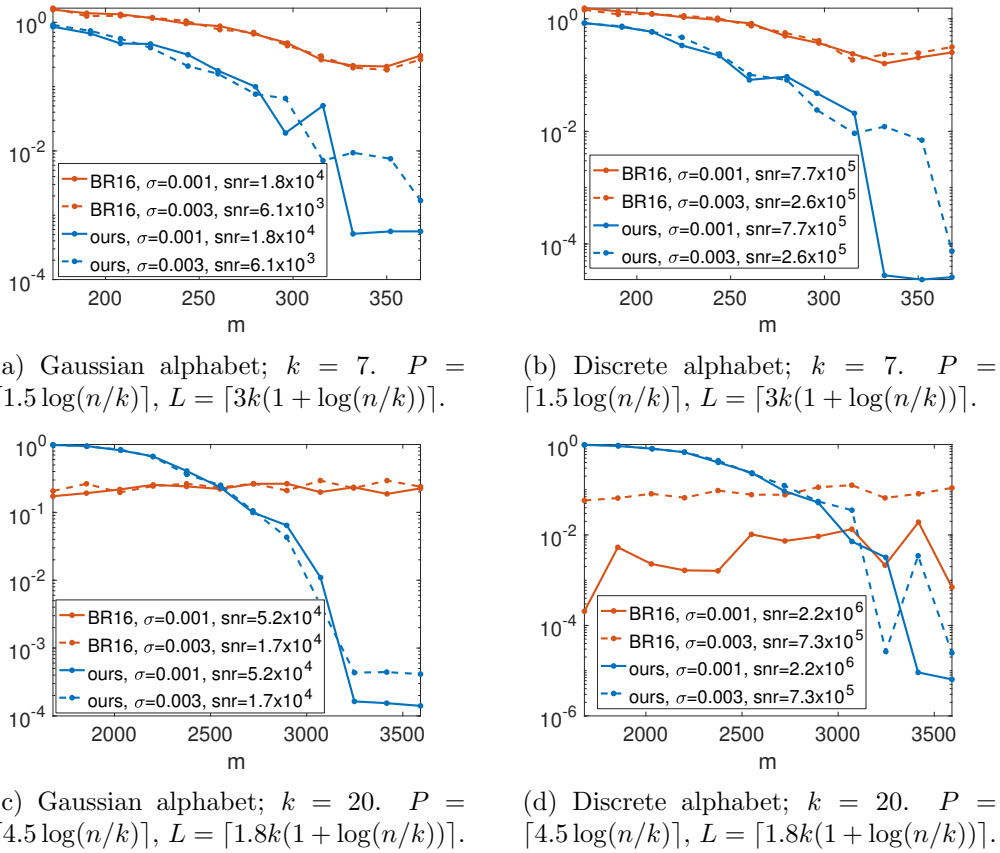


Figure 11: Normalized error $\|\hat{\mathbf{X}}_0 - \mathbf{X}_0\|_F / \|\mathbf{X}_0\|_F$ of our scheme (red lines) and the nested sketching scheme proposed in [33, 35] (blue lines) plotted against m . In each setting, \mathbf{X}_0 is a 100×100 rank-2 PSD matrix, whose eigenvectors have disjoint supports. The solid and dashed lines correspond to $\sigma = 0.001$ and $\sigma = 0.003$. SNR is $\lambda/(\sqrt{n}\sigma)$. $\gamma_0 = 5, \gamma_1 = 2.5$. Results are averaged over 60 trials.

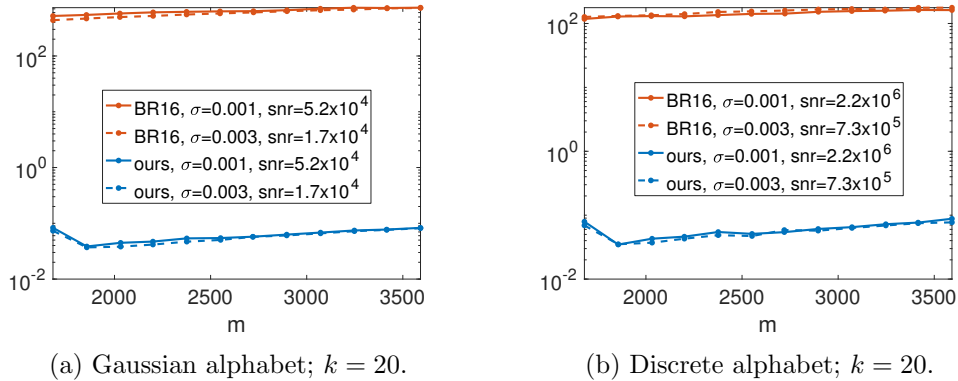


Figure 12: Running time of our scheme (red lines) and the nested sketching scheme (blue lines), recorded in the experiments for Figs. 11c–11d. Results are averaged over 60 trials.

11c–11d), our scheme needs more measurements to go through phase transition in normalized error. Nevertheless, it achieves an error that’s 2 to 4 orders of magnitude smaller than the latter after the transition. We note that the normalized error of the nested scheme is on the order of 10^{-1} , which agrees with the simulation results in [35, Sec. III].

The nested sketching scheme was implemented according to the description in [33, Sec. 4]. We used TFOCS [44] for the low-rank estimation stage (35) and a variant of the Alternating Direction Method of Multipliers adapted from [46, 47] for the sparse estimation stage (36). This implementation is significantly faster than that via CVX, but as shown in Fig. 12, is still on average 3 to 4 orders of magnitude slower than our algorithm.

5 Proofs of main lemmas

In this section, we give the proofs of Lemmas 3.1–3.4.

5.1 Preliminaries

We begin with the following tail bound for binomial random variables, which follows from Sanov’s theorem [48, Theorem 12.4.1].

Lemma 5.1 (Tail bound for Binomial). *For $X \sim \text{Bin}(n, p)$,*

$$\mathbb{P}\{X \leq x\} \leq \exp\left(-nD_e\left(\frac{x}{n}\middle\|p\right)\right) \quad \text{for } 0 \leq x \leq np, \quad (37)$$

$$\mathbb{P}\{X \geq x\} \leq \exp\left(-nD_e\left(\frac{x}{n}\middle\|p\right)\right) \quad \text{for } np \leq x \leq n, \quad (38)$$

where $D_e(q\|p) := q \ln \frac{q}{p} + (1 - q) \ln \frac{1-q}{1-p}$.

We will use the notion of *negative association* (NA) [26, 49] to handle the dependence between the degrees of the bipartite graphs we analyze. Roughly speaking, a collection of random variables X_1, X_2, \dots, X_n are negatively associated if whenever a subset of them is high, then a disjoint subset of them must be low.

Definition 5.1 (Negative Association (NA)). *The random variables X_1, X_2, \dots, X_n are said to be negatively associated if for any two disjoint index sets $\mathcal{I}, \mathcal{J} \subseteq [n]$ and two functions $f : \mathbb{R}^{|\mathcal{I}|} \rightarrow \mathbb{R}$, $g : \mathbb{R}^{|\mathcal{J}|} \rightarrow \mathbb{R}$ both monotonically increasing or monotonically decreasing,*

$$\mathbb{E}[f(X_i, i \in \mathcal{I})g(X_j, j \in \mathcal{J})] \leq \mathbb{E}[f(X_i, i \in \mathcal{I})] \mathbb{E}[g(X_j, j \in \mathcal{J})]. \quad (39)$$

Lemma 5.2 (Useful properties of NA [26, 49]).

- (i) *The union of independent sets of NA random variables is NA.*
- (ii) *Concordant monotone functions (i.e., all monotonically increasing or all monotonically decreasing functions) defined on disjoint subsets of a set of NA random variables are NA.*
- (iii) *Let $\mathbf{x} = [x_1, x_2, \dots, x_n]$ be a real-valued vector and let $\mathbf{X} = [X_1, X_2, \dots, X_n]$ be a random vector which takes as values all the $n!$ permutations of \mathbf{x} with equal probabilities. Then X_1, X_2, \dots, X_n are NA.*

Lemma 5.3 (Chernoff bound for NA Bernoulli variables [26]). *Let X_1, X_2, \dots, X_n be NA random variables with $X_i \in \{0, 1\}$ for $i \in [n]$. Then, $Y = \sum_{i=1}^n X_i$ satisfies:*

$$\mathbb{P}\{Y > (1 + \epsilon)\mathbb{E}[Y]\} \leq \exp\left(-\frac{\epsilon^2 \mathbb{E}[Y]}{2 + \epsilon}\right) \quad \text{for any } \epsilon \geq 0, \quad (40)$$

$$\mathbb{P}\{Y < (1 - \epsilon)\mathbb{E}[Y]\} \leq \exp\left(-\frac{\epsilon^2 \mathbb{E}[Y]}{2 - \epsilon}\right) \quad \text{for any } \epsilon \in [0, 1]. \quad (41)$$

5.2 Proof of Lemma 3.1

The pruned graph at the start of stage A has $r\tilde{k} = r\binom{k}{2} + k$ left nodes, each with d edges. Fig. 1a is an example for $r = 1$. The number of right nodes is $R = dr\tilde{k}/(\delta \ln k)$. Let Z_j denote the degree of the j -th right node for $j \in [R]$. Since the total number of edges in the graph is $dr\tilde{k}$, we have $\sum_{j=1}^R Z_j = dr\tilde{k}$.

Lemma 5.4 (Initial right degrees are Binomial and NA). *For $j \in [R]$, we have $Z_j \sim \text{Bin}\left(r\tilde{k}, \frac{d}{R}\right)$. Furthermore, Z_1, Z_2, \dots, Z_R are NA.*

Proof. Recall that the bipartite graph at the start of stage A for a rank- r matrix \mathbf{X} has $r\tilde{k}$ left nodes and R right nodes. For $l \in [r\tilde{k}]$ and $j \in [R]$, let

$$Y_{l,j} := \begin{cases} 1 & \text{if the } l\text{-th left node connects to the } j\text{-th right node,} \\ 0 & \text{otherwise.} \end{cases} \quad (42)$$

Observe that $Y_{l,j} \sim \text{Bern}\left(\frac{d}{R}\right)$ and that $Y_{l_1, j_1} \perp Y_{l_2, j_2}$ for $l_1 \neq l_2$. Therefore,

$$Z_j = \sum_{l=1}^{r\tilde{k}} Y_{l,j} \sim \text{Bin}\left(r\tilde{k}, \frac{d}{R}\right) \quad \text{for } j \in [R]. \quad (43)$$

By the construction of the bipartite graph, the vector $\mathbf{Y}_l := [Y_{l,1}, Y_{l,2}, \dots, Y_{l,R}]$ contains d ones, distributed uniformly at random among its R entries; the remaining $(R - d)$ entries are

zeros. That is, the joint distribution of the entries of \mathbf{Y}_l is a permutation distribution. Hence, $[Y_{l,1}, Y_{l,2}, \dots, Y_{l,R}]$ is NA by Lemma 5.2(iii). Since the vectors \mathbf{Y}_l are mutually independent for $l \in [r\tilde{k}]$, the concatenated vector $[Y_{l,j} \forall l \in [r\tilde{k}], \forall j \in [R]]$ is NA by Lemma 5.2(i). Furthermore, from (43), we note that Z_1, \dots, Z_R are increasing functions defined on disjoint subsets of the $Y_{l,j}$'s. Thus, by Lemma 5.2(ii), Z_1, \dots, Z_R are NA. \square

The number of left nodes (i.e. nonzero matrix entries) recovered in stage A is at least as large as the number of singletons at the start of stage A, which equals $\sum_{j=1}^R \mathbb{1}\{Z_j = 1\}$. We now use Lemma 5.4 to obtain a high probability bound on this sum.

Lemma 5.5 (Bound on number of singletons). *Let $Z \sim \text{Bin}\left(r\tilde{k}, \frac{d}{R}\right)$. Then, for sufficiently large k , the number of singletons $\sum_{j=1}^R \mathbb{1}\{Z_j = 1\}$ satisfies:*

$$\mathbb{P}\left\{\left|\frac{1}{R}\sum_{j=1}^R \mathbb{1}\{Z_j = 1\} - \mathbb{P}\{Z = 1\}\right| \geq k^{-\delta}\right\} < 4 \exp\left(-\frac{dr}{17\delta^2} \frac{k^{2-\delta}}{\ln^2 k}\right). \quad (44)$$

Proof. We first note

$$\frac{1}{R}\sum_{j=1}^R \mathbb{1}\{Z_j = 1\} - \mathbb{P}\{Z = 1\} = \frac{1}{R}\sum_{j=1}^R \mathbb{1}\{Z_j \leq 1\} - \mathbb{P}\{Z \leq 1\} + \mathbb{P}\{Z = 0\} - \frac{1}{R}\sum_{j=1}^R \mathbb{1}\{Z_j = 0\}.$$

Applying the triangle inequality and a union bound, we have

$$\begin{aligned} & \mathbb{P}\left\{\left|\frac{1}{R}\sum_{j=1}^R \mathbb{1}\{Z_j = 1\} - \mathbb{P}\{Z = 1\}\right| \geq k^{-\delta}\right\} \\ & \leq \mathbb{P}\left\{\left|\frac{1}{R}\sum_{j=1}^R \mathbb{1}\{Z_j \leq 1\} - \mathbb{P}\{Z \leq 1\}\right| \geq \frac{k^{-\delta}}{2}\right\} + \mathbb{P}\left\{\left|\frac{1}{R}\sum_{j=1}^R \mathbb{1}\{Z_j = 0\} - \mathbb{P}\{Z = 0\}\right| \geq \frac{k^{-\delta}}{2}\right\}. \end{aligned} \quad (45)$$

For brevity, denote the two terms in (45) by T_1 and T_2 , respectively. Since Z_1, \dots, Z_R are NA (by Lemma 5.4) and $\mathbb{1}\{Z_j \leq 1\}$ is monotonic in Z_j , by Lemma 5.2(ii), the random variables $\mathbb{1}\{Z_j \leq 1\}$ for $j \in [R]$ are NA. Thus, applying the Chernoff bound in Lemma 5.3 and recalling that $R = dr\tilde{k}/(\delta \ln k)$, we obtain that for sufficiently large k

$$T_1 \leq 2 \exp\left(-\frac{R}{2(2k^\delta)^2 \mathbb{P}\{Z \leq 1\} (1 + o(1))}\right) < 2 \exp\left(-\frac{dr}{17\delta^2} \frac{k^{2-\delta}}{\ln^2 k}\right), \quad (46)$$

where we have used the fact that $\mathbb{P}\{Z = 0\} = k^{-\delta}(1 - o(1))$ and $\mathbb{P}\{Z = 1\} = (\delta \ln k)k^{-\delta}(1 - o(1))$. Similarly, using that $\mathbb{1}\{Z_j = 0\}$ is monotonic in Z_j , we deduce that

$$T_2 \leq 2 \exp\left(-\frac{R}{2(2k^\delta)^2 \mathbb{P}\{Z = 0\} (1 + o(1))}\right) < 2 \exp\left(-\frac{dr}{17\delta} \frac{k^{2-\delta}}{\ln k}\right). \quad (47)$$

Combining the upper bounds on T_1 and T_2 yields (44). \square

We now prove (13) from (44). Using $R = dr\tilde{k}/(\delta \ln k)$ and $\mathbb{P}\{Z = 1\} = (\delta \ln k)k^{-\delta}(1 - o(1))$, we deduce from (44) that there exists a non-negative sequence $c_{k,\delta} = o(1)$ such that for sufficiently large k ,

$$\mathbb{P}\left\{\sum_{j=1}^R \mathbb{1}\{Z_j = 1\} \leq dr\tilde{k} \cdot k^{-\delta}(1 - c_{k,\delta})\right\} < 4 \exp\left(-\frac{dr}{17\delta^2} \frac{k^{2-\delta}}{\ln^2 k}\right). \quad (48)$$

Since each left node connects to at most d singletons, the number of left nodes recoverable from just the singletons in the initial graph is at least $\frac{1}{d} \sum_{j=1}^R \mathbb{1}\{Z_j = 1\}$. This number is smaller than the total number of left nodes recoverable in stage A because additional singletons may be created during the peeling process. Thus, with \mathbf{A} denoting the total fraction of left nodes (out of $r\tilde{k}$) recovered in stage A, using (48) we have:

$$\begin{aligned} \mathbb{P}\left\{Ar\tilde{k} \leq r\tilde{k}k^{-\delta}(1 - c_{k,\delta})\right\} &\leq \mathbb{P}\left\{\frac{1}{d} \sum_{j=1}^R \mathbb{1}\{Z_j = 1\} \leq r\tilde{k}k^{-\delta}(1 - c_{k,\delta})\right\} \\ &< 4 \exp\left(-\frac{dr}{17\delta^2} \frac{k^{2-\delta}}{\ln^2 k}\right). \end{aligned} \quad (49)$$

Rearranging (49) yields (13).

We now prove (14). For $l \in [r\tilde{k}]$, let

$$\bar{V}_l := \begin{cases} 1 & \text{if the } l\text{-th left node is recovered by the end of stage A,} \\ 0 & \text{otherwise.} \end{cases} \quad (50)$$

Since the recovered left nodes are distributed uniformly at random among all left nodes, each $\bar{V}_l \sim \text{Bern}(\mathbf{A})$. Moreover, conditioned on $\sum_{l=1}^{r\tilde{k}} \bar{V}_l = Ar\tilde{k}$, the $\{\bar{V}_l\}$ are NA by Lemma 5.2(iii). Let \mathcal{S}_{Di} and \mathcal{S}_i be the set of indices of the left nodes that represent the diagonal and above-diagonal entries in the i -th nonzero submatrix (corresponding to $\lambda_i \mathbf{v}_i \mathbf{v}_i^T$), respectively, with $|\mathcal{S}_{Di}| = k$ and $|\mathcal{S}_i| = \binom{k}{2}$.

The number of diagonal entries (out of k) recovered in the i -th nonzero submatrix is $N_{Di} = \sum_{l \in \mathcal{S}_{Di}} \bar{V}_l$, which can be bounded as follows using the Chernoff bound in Lemma 5.3. Recalling that $\alpha^* = k^{-\delta} - o(k^{-\delta})$, we have for any fixed $\epsilon \in (0, \frac{1}{5})$ and sufficiently large k ,

$$\begin{aligned} \mathbb{P}\{N_{Di} < 1 \mid \mathbf{A} = \alpha^*\} &\leq \mathbb{P}\{N_{Di} < k\alpha^*\epsilon \mid \mathbf{A} = \alpha^*\} \\ &\leq \mathbb{P}\left\{\sum_{l \in \mathcal{S}_{Di}} \bar{V}_l < k\mathbb{E}[\bar{V}_l \mid \mathbf{A}]\epsilon \mid \mathbf{A} = \alpha^*\right\} \\ &\leq \exp\left(-\frac{(1-\epsilon)^2 k\alpha^*}{1+\epsilon}\right) \leq \exp\left(-\frac{1}{2}k^{1-\delta}\right). \end{aligned} \quad (51)$$

The fraction of above-diagonal entries (out of $\binom{k}{2}$) recovered in the i -th nonzero submatrix is $\mathbf{A}_i = \frac{1}{\binom{k}{2}} \sum_{l \in \mathcal{S}_i} \bar{V}_l$. Let $\alpha_i^* = \alpha^*(1 - k^{-\frac{1}{4}})$. Then using the Chernoff bound in Lemma 5.3, we have

for sufficiently large k ,

$$\begin{aligned}
\mathbb{P}\{A_i < \alpha_i^* \mid A = \alpha^*\} &= \mathbb{P}\left\{\frac{1}{\binom{k}{2}} \sum_{l \in \mathcal{S}_i} \bar{V}_l < \alpha^* \left(1 - k^{-\frac{1}{4}}\right) \mid A = \alpha^*\right\} \\
&= \mathbb{P}\left\{\frac{1}{\binom{k}{2}} \sum_{l \in \mathcal{S}_i} \bar{V}_l < \mathbb{E}[\bar{V}_l \mid A] \left(1 - k^{-\frac{1}{4}}\right) \mid A = \alpha^*\right\} \\
&\leq \exp\left(-\frac{\left(k^{-\frac{1}{4}}\right)^2 \binom{k}{2} \alpha^*}{2}\right) \leq \exp\left(-\frac{1}{8} k^{\frac{3}{2}-\delta}\right). \tag{52}
\end{aligned}$$

Finally, we obtain (14) using (51) and (52) as follows. For sufficiently large k , we have

$$\begin{aligned}
&\mathbb{P}\{N_{D_i} \geq 1 \text{ and } A_i \geq \alpha_i^*, \forall i \in [r]\} \\
&\geq \mathbb{P}\{A \geq \alpha^*\} \mathbb{P}\{N_{D_i} \geq 1 \text{ and } A_i \geq \alpha_i^*, \forall i \in [r] \mid A = \alpha^*\} \\
&\stackrel{(i)}{\geq} \mathbb{P}\{A \geq \alpha^*\} \left[1 - \sum_{i=1}^r \mathbb{P}\{N_{D_i} < 1 \mid A = \alpha^*\} - \sum_{i=1}^r \mathbb{P}\{A_i < \alpha_i^* \mid A = \alpha^*\}\right] \\
&\stackrel{(ii)}{\geq} \left[1 - 4 \exp\left(-\frac{dr}{17\delta^2} \frac{k^{2-\delta}}{\ln^2 k}\right)\right] \left[1 - r \exp\left(-\frac{1}{2} k^{1-\delta}\right) - r \exp\left(-\frac{1}{8} k^{\frac{3}{2}-\delta}\right)\right] \\
&\geq 1 - 2r \exp\left(-\frac{1}{2} k^{1-\delta}\right), \tag{53}
\end{aligned}$$

where (i) is obtained using a union bound, and (ii) by applying (13), (51) and (52). \square

5.3 Proof of Lemma 3.2

Since the eigenvectors $\{\mathbf{v}_1, \dots, \mathbf{v}_r\}$ have non-overlapping supports, the nonzero entries of $\mathbf{X} = \sum_{i=1}^r \lambda_i \mathbf{v}_i \mathbf{v}_i^T$ form r disjoint submatrices, each of size $k \times k$. Therefore, the graph for stage B consists of r disjoint bipartite subgraphs, one corresponding to each submatrix. Specifically, the i -th subgraph has k left nodes representing the unknown nonzeros in the i -th eigenvector and $A_i \binom{k}{2}$ right nodes representing the nonzero pairwise products recovered in the i -th submatrix in stage A. (See Fig. 2a for an example subgraph.) The peeling algorithm described in Section 2.2.2 is applied to each of these subgraphs.

Consider the i -th subgraph, given A_i and the event that $N_{D_i} \geq 1$. The $A_i \binom{k}{2}$ right nodes can be seen as drawn uniformly at random without replacement from the $\binom{k}{2}$ nonzero pairwise products in the i -th submatrix. This creates dependence between the degrees of the left nodes, which makes the evolution of the random graph process in Fig. 2 difficult to characterize. We therefore consider an alternative graph process, in which the $A_i \binom{k}{2}$ right nodes at the start of stage B are drawn uniformly at random *with replacement* from the $\binom{k}{2}$ nonzero pairwise products in the i -th submatrix; see Fig. 13a for an illustration. Stage B of the algorithm proceeds in the same way on the alternative graph as the original. At $t = 0$, a left node is recovered based on one of the nonzero diagonal entries recovered in stage A (Fig. 13b). Then, for each $t \geq 1$, a degree-1 right node is picked uniformly at random from the available ones and its connecting left node recovered and peeled off to update the

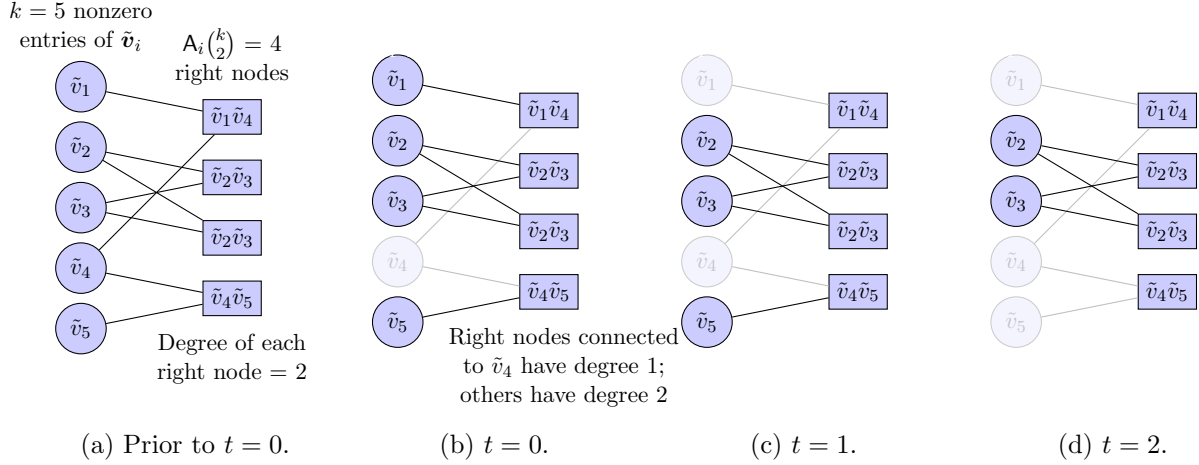


Figure 13: Alternative graph process showing the recovery of $\tilde{\mathbf{v}}_i$ for $\mathbf{X} = \sum_{i=1}^r \tilde{\mathbf{v}}_i \tilde{\mathbf{v}}_i^T$ given A_i and $N_{Di} \geq 1$ (as the counterpart of Fig. 2). The double occurrence of $\tilde{v}_2\tilde{v}_3$ as right nodes highlights that the right nodes are sampled *with replacement* from the $\binom{k}{2}$ nonzero pairwise products in the nonzero submatrix corresponding to $\tilde{\mathbf{v}}_i \tilde{\mathbf{v}}_i^T$. The faded nodes and edges are those that have been peeled off.

set of degree-1 right nodes. This continues till there are no more degree-1 right nodes (Figs. 13c and 13d).

Since the right nodes in the alternative graph are sampled with replacement, the number of distinct right nodes in the alternative graph at the start of stage B can be no larger than $A_i \binom{k}{2}$. Any repeated right nodes do not play a role in the recovery algorithm. Let $B_{\text{alt},i}$ denote the fraction of left nodes recovered when there remain no degree-1 right nodes in the alternative graph process. Since the number of distinct right nodes in the initial alternative graph is no larger than that in the original one, we have:

$$\mathbb{P}\{B_{\text{alt},i} < 1 \mid N_{Di}, A_i\} \geq \mathbb{P}\{B_i < 1 \mid N_{Di}, A_i\}, \quad i \in [r], \quad \forall N_{Di} \geq 1, A_i \geq \alpha_i^*. \quad (54)$$

We will prove (15) by showing that

$$\mathbb{P}\{B_{\text{alt},i} < 1 \mid N_{Di}, A_i\} < \exp\left(-\frac{1}{30}k^{1-\delta}\right), \quad i \in [r], \quad \forall N_{Di} \geq 1, A_i \geq \alpha_i^*. \quad (55)$$

For brevity, we shall refer to ‘prior to $t = 0$ ’ as ‘at $t = -1$ ’. Given A_i , let \tilde{Z}_l be the degree of the l -th left node in the alternative graph at $t = -1$ (i.e. Fig. 13a), for $l \in [k]$. Since each right node has degree-2 at $t = -1$, the total number of edges at $t = -1$ is $\sum_{l=1}^k \tilde{Z}_l = 2A_i \binom{k}{2}$.

Lemma 5.6 (Initial left degrees are Binomial). *For $l \in [k]$,*

$$\tilde{Z}_l \sim \text{Bin}\left(A_i \binom{k}{2}, \frac{2}{k}\right). \quad (56)$$

Let

$$\mu := A_i \binom{k}{2} \frac{2}{k} = A_i(k-1). \quad (57)$$

Then, for $A_i \geq \alpha_i^*$, we have for sufficiently large k ,

$$\mathbb{P} \left\{ \tilde{Z}_l \leq \frac{\mu}{2} \right\} < \exp \left(-\frac{1}{10} k^{1-\delta} \right), \quad \mathbb{P} \left\{ \tilde{Z}_l \geq \frac{3\mu}{2} \right\} < \exp \left(-\frac{1}{10} k^{1-\delta} \right). \quad (58)$$

Proof. The result (56) follows from a standard counting argument, noting that the right nodes are picked uniformly at random with replacement and that each right node has degree 2 at $t = -1$. Result (58) is obtained using the Binomial tail bound in Lemma 5.1 and simplifying the resulting expression. \square

Recall that one left node is recovered in each iteration $t \geq 0$ of the peeling algorithm, until there are no more degree-1 right nodes left. Let $\pi(t)$ denote the index of the left node recovered in iteration t . Thus, $\pi : \{0, 1, \dots, k-1\} \rightarrow \{1, 2, \dots, k\}$. If the decoding process has not terminated after iteration $(t-1)$, for $1 \leq t \leq (k-1)$, then t left nodes out of k have been peeled off. For the algorithm to proceed, we need at least one of the remaining $(k-t)$ left nodes to be connected to at least one degree-1 right node. The following lemma obtains the distribution of the number of degree-1 right nodes connected to each remaining left node, after each iteration of the peeling algorithm.

Lemma 5.7 (Number of degree-1 right nodes connected to each unpeeled left node). *Consider the alternative graph process on subgraph $i \in [r]$, given A_i and N_{D_i} . Suppose that the peeling algorithm on this subgraph has not terminated after iteration $(t-1)$, for $1 \leq t \leq (k-1)$. Let $S_l^{(t)}$ be the number of degree-1 right nodes connected to the l -th remaining left node at the start of iteration t , for $l \in [k] \setminus \{\pi(0), \dots, \pi(t-1)\}$. Then*

$$S_l^{(t)} \sim \text{Bin} \left(A_i \binom{k}{2}, \frac{t}{\binom{k}{2}} \right). \quad (59)$$

Moreover, for $A_i \geq \alpha_i^*$ and sufficiently large k , the following holds for $1 \leq t \leq \frac{k-1}{20}$:

$$\mathbb{P} \left\{ S_l^{(t)} \geq \frac{\mu}{5} \mid S_l^{(t)} \geq 1 \right\} < \exp \left(-\frac{1}{16} k^{1-\delta} \right), \quad (60)$$

where $\mu = A_i(k-1)$ as defined in (57).

Proof. For $l \in [k]$ and $j \in [A_i \binom{k}{2}]$, let

$$Y_{l,j} := \begin{cases} 1 & \text{if the } l\text{-th left node connects to the } j\text{-th right node at } t = -1, \\ 0 & \text{otherwise.} \end{cases} \quad (61)$$

At $t = -1$, since each right node has degree 2 (see Fig. 13a), the vector $[Y_{1,j}, Y_{2,j}, \dots, Y_{k,j}]$ contains exactly two ones distributed uniformly at random, and the remaining entries are zero. It follows that $\sum_{l=1}^k Y_{l,j} = 2$, $Y_{l,j} \sim \text{Bern} \left(\frac{2}{k} \right)$ and $Y_{l_1,j} \cdot Y_{l_2,j} \sim \text{Bern} \left(1/\binom{k}{2} \right)$ for $l_1 \neq l_2$. Moreover, by construction of the alternative graph, the edges of each right node are independent from those of the others, so $Y_{l_1,j_1} \perp Y_{l_2,j_2}$ for $j_1 \neq j_2$.

In iteration $t = 0$, the first left node $v_{\pi(0)}$ is peeled off. Consider one of the $(k-1)$ remaining left nodes after iteration $t = 0$, say v_l . The number of degree-1 right nodes connected to v_l is equal

to the number of right nodes which were connected to v_l and $v_{\pi(0)}$ at $t = -1$. That is, at the start of iteration $t = 1$, we have

$$S_l^{(1)} = \sum_{j=1}^{A_i \binom{k}{2}} Y_{l,j} \cdot Y_{\pi(0),j} \stackrel{(i)}{\sim} \text{Bin} \left(A_i \binom{k}{2}, \frac{1}{\binom{k}{2}} \right), \quad l \in [k] \setminus \pi(0), \quad (62)$$

where (i) holds because $Y_{l,j} \cdot Y_{\pi(0),j} \stackrel{\text{iid}}{\sim} \text{Bern}(1/\binom{k}{2})$ for $l \neq \pi(0)$ and $j \in [A_i \binom{k}{2}]$.

More generally, when t left nodes have been peeled off by the end of iteration $(t - 1)$, consider one of the remaining left nodes, say v_l . Then the number of degree-1 right nodes connected to v_l is the number of right nodes which were originally connected to v_l and some recovered v_ι , i.e., v_ι for $\iota \in \{\pi(0), \dots, \pi(t - 1)\}$. Hence, we deduce that

$$S_l^{(t)} = \sum_{j=1}^{A_i \binom{k}{2}} \sum_{\kappa=0}^{t-1} Y_{l,j} \cdot Y_{\pi(\kappa),j} \stackrel{(i)}{\sim} \text{Bin} \left(A_i \binom{k}{2}, \frac{t}{\binom{k}{2}} \right), \quad l \in [k] \setminus \{\pi(0), \dots, \pi(t - 1)\}, \quad (63)$$

where (i) is obtained by noting that for $l \notin \{\pi(0), \dots, \pi(t - 1)\}$ and each j , the sum $\sum_{\kappa=0}^{t-1} Y_{l,j} Y_{\pi(\kappa),j} \sim \text{Bern}(t/\binom{k}{2})$, and that these sums are mutually independent across $j \in [A_i \binom{k}{2}]$. This gives the result in (59).

We next prove (60) for $A_i \geq \alpha_i^*$ using the distribution in (59). For $1 \leq t \leq \frac{k-1}{20}$ and sufficiently large k , applying the Binomial tail bound in Lemma 5.1, we obtain

$$\begin{aligned} \mathbb{P} \left\{ S_l^{(t)} \geq \frac{\mu}{5} \mid S_l^{(t)} \geq 1 \right\} &\leq \frac{\exp \left(-A_i \binom{k}{2} D_e \left(\frac{\mu/5}{A_i \binom{k}{2}} \parallel \frac{t}{\binom{k}{2}} \right) \right)}{1 - \left(1 - t/\binom{k}{2} \right)^{A_i \binom{k}{2}}} \\ &\leq \frac{\exp \left(-A_i \binom{k}{2} D_e \left(\frac{\mu/5}{A_i \binom{k}{2}} \parallel \frac{(k-1)/20}{\binom{k}{2}} \right) \right)}{1 - \left(1 - 1/\binom{k}{2} \right)^{A_i \binom{k}{2}}} \\ &\stackrel{(i)}{<} \frac{\exp(-k^{1-\delta}/8)}{\alpha_i^*/2} < \exp \left(-\frac{1}{16} k^{1-\delta} \right). \end{aligned} \quad (64)$$

For the inequality (i), the numerator is obtained by simplifying the relative entropy term and noting that $A_i \geq \alpha_i^*$; the denominator is obtained using $(1 - 1/\binom{k}{2})^{A_i \binom{k}{2}} \leq (1 - 1/\binom{k}{2})^{\alpha_i^* \binom{k}{2}} \leq e^{-\alpha_i^*} < 1 - \alpha_i^*/2$ (where the last step holds since $\alpha_i^* \in (0, 1)$). \square

Lemma 5.8 (Degree-1 right nodes don't run out in initial iterations). *Consider the alternative graph process on subgraph $i \in [r]$, given $A_i \geq \alpha_i^*$ and $N_{D_i} \geq 1$. Let $C_1(t) \in \mathbb{N}_0$ denote the number of degree-1 right nodes in the residual subgraph after iteration t of the peeling algorithm. Let $t_0 := \frac{k-1}{20}$, and define the event*

$$\mathcal{E} := \{C_1(t) > 0, \text{ for } 0 \leq t \leq t_0\}. \quad (65)$$

Then, for sufficiently large k ,

$$\mathbb{P} \{ \mathcal{E} \} > 1 - \exp \left(-\frac{1}{20} k^{1-\delta} \right). \quad (66)$$

Proof. Recall that the initial left degrees (at $t = -1$), denoted by $\{\tilde{Z}_l\}_{l \in [k]}$, each has a Binomial distribution given in (56). Recall also that $\pi(t)$ is the index of the left node recovered in iteration t . At $t = 0$, the first left node $v_{\pi(0)}$ is peeled off, creating $\tilde{Z}_{\pi(0)}$ degree-1 right nodes. Thus, we have

$$C_1(0) = \tilde{Z}_{\pi(0)}. \quad (67)$$

More generally, after iteration $(t - 1)$, when t left nodes have been peeled off, consider one of the $(k - t)$ remaining left nodes, say v_l , for some $l \in [k] \setminus \{\pi(0), \dots, \pi(t - 1)\}$. At the start of iteration t , among the \tilde{Z}_l edges of v_l , the number of edges connected to degree-1 right nodes is $S_l^{(t)}$ whose distribution is given in (59). When one of the $(k - t)$ remaining left nodes, denoted by $v_{\pi(t)}$, is peeled off in iteration t , the number of degree-1 right nodes in the residual graph can be expressed as:

$$\begin{aligned} C_1(t) &= C_1(t - 1) + \# \text{ degree-2 right nodes reduced to degree-1 due to the removal of } v_{\pi(t)} \\ &\quad - \# \text{ degree-1 right nodes reduced to degree-0 due to the removal of } v_{\pi(t)} \\ &= C_1(t - 1) + \left(\tilde{Z}_{\pi(t)} - S_{\pi(t)}^{(t)} \right) - S_{\pi(t)}^{(t)} \\ &= C_1(t - 1) + \left(\tilde{Z}_{\pi(t)} - 2S_{\pi(t)}^{(t)} \right). \end{aligned} \quad (68)$$

The marginal distributions of $\tilde{Z}_{\pi(t)}$ and $S_{\pi(t)}^{(t)}$ are given by Lemmas 5.6 and 5.7, which also guarantee that with high probability, $\tilde{Z}_{\pi(t)} > \frac{\mu}{2}$ and $S_{\pi(t)}^{(t)} < \frac{\mu}{5}$ for $t \leq t_0$.

By the same reasoning as above, we can write $C_1(t - 1)$ in terms of $C_1(t - 2)$ and so on to obtain

$$\begin{aligned} C_1(t) &= C_1(t - 1) + \left(\tilde{Z}_{\pi(t)} - 2S_{\pi(t)}^{(t)} \right) \\ &= C_1(0) + \sum_{\kappa=1}^t \left(\tilde{Z}_{\pi(\kappa)} - 2S_{\pi(\kappa)}^{(\kappa)} \right) \\ &= \tilde{Z}_{\pi(0)} + \sum_{\kappa=1}^t \left(\tilde{Z}_{\pi(\kappa)} - 2S_{\pi(\kappa)}^{(\kappa)} \right), \end{aligned} \quad (69)$$

where the last step follows from (67). We next show that $C_1(t) > 0$ with high probability for $0 \leq t \leq t_0$ by bounding each term on the RHS of (69). From (69), we note that

$$\begin{aligned} \left\{ \tilde{Z}_{\pi(t)} > \frac{\mu}{2} \text{ and } S_{\pi(t)}^{(t)} < \frac{\mu}{5}, \forall t \leq t_0 \right\} &\Rightarrow \left\{ C_1(t) > \frac{\mu}{2} + t \left(\frac{\mu}{2} - \frac{2\mu}{5} \right), \forall t \in [0, t_0] \right\} \\ &\Rightarrow \{C_1(t) > 0, \forall t \in [0, t_0]\}. \end{aligned} \quad (70)$$

It follows that

$$\begin{aligned} \mathbb{P}\{\mathcal{E}\} &= \mathbb{P}\{C_1(t) > 0, \forall t \in [0, t_0]\} \\ &\geq \mathbb{P}\left\{ \tilde{Z}_{\pi(t)} > \frac{\mu}{2} \text{ and } S_{\pi(t)}^{(t)} < \frac{\mu}{5}, \forall t \leq t_0 \mid S_{\pi(t)}^{(t)} \geq 1, \forall t \in [1, t_0] \right\}, \end{aligned} \quad (71)$$

where the condition $S_{\pi(t)}^{(t)} \geq 1, \forall t \in [1, t_0]$ captures the fact that the left node recovered in each iteration t was connected to at least one degree-1 right node at t . Applying a union bound gives

$$\mathbb{P}\{\mathcal{E}\} \geq 1 - \sum_{t=0}^{t_0} \mathbb{P}\left\{ \tilde{Z}_{\pi(t)} \leq \frac{\mu}{2} \right\} - \sum_{t=1}^{t_0} \mathbb{P}\left\{ S_{\pi(t)}^{(t)} \geq \frac{\mu}{5} \mid S_{\pi(t)}^{(t)} \geq 1 \right\}. \quad (72)$$

Each summand in the second term can be bounded using (58) and each summand in the third term can be bounded using (60) for $t \leq t_0 = \frac{k-1}{20}$. We therefore obtain

$$\begin{aligned} \mathbb{P}\{\mathcal{E}\} &> 1 - (t_0 + 1) \exp\left(-\frac{1}{10}k^{1-\delta}\right) - t_0 \exp\left(-\frac{1}{16}k^{1-\delta}\right) \\ &> 1 - \left(\frac{k-1}{20} + 1\right) \exp\left(-\frac{1}{10}k^{1-\delta}\right) - \frac{k-1}{20} \exp\left(-\frac{1}{16}k^{1-\delta}\right) \\ &> 1 - \exp\left(-\frac{1}{20}k^{1-\delta}\right), \end{aligned} \quad (73)$$

where the last inequality holds for sufficiently large k . \square

We now prove Lemma 3.2 by proving (55) based on Lemmas 5.7 and 5.8. In particular, we show that after $t_0 = \frac{k-1}{20}$ iterations, every remaining left node in the residual subgraph is connected to at least one degree-1 right node with high probability and so can be recovered by the peeling algorithm.

Proof of Lemma 3.2. Consider the alternative graph process on subgraph $i \in [r]$. Conditioned on the event

$$\mathcal{E} = \{C_1(t) > 0, \forall t \in [0, t_0]\},$$

$(t_0 + 1)$ left nodes (out of k) have been recovered and peeled off by iteration t_0 . Consider one of the remaining left nodes after iteration t_0 , i.e., v_l with $l \in [k] \setminus \{\pi(0), \dots, \pi(t_0)\}$. We show that with high probability, v_l is connected to at least one degree-1 right node and is therefore recoverable in the forthcoming steps. From Lemma 5.7, the number of degree-1 right nodes connected to v_l after iteration t_0 , denoted by $S_l^{(t_0+1)}$, is distributed as $S_l^{(t_0+1)} \sim \text{Bin}\left(\mathbf{A}_i \binom{k}{2}, (t_0 + 1)/\binom{k}{2}\right)$. Thus, using $t_0 = \frac{k-1}{20}$ and $\mathbf{A}_i \geq \alpha_i^*$, we have the bound

$$\mathbb{P}\left\{S_l^{(t_0+1)} = 0 \mid \mathcal{E}\right\} = \left(1 - \frac{t_0 + 1}{\binom{k}{2}}\right)^{\mathbf{A}_i \binom{k}{2}} \leq \exp(-(t_0 + 1)\alpha_i^*) < \exp\left(-\frac{1}{25}k^{1-\delta}\right). \quad (74)$$

Applying a union bound gives

$$\begin{aligned} \mathbb{P}\left\{S_l^{(t_0+1)} \geq 1, \forall l \in [k] \setminus \{\pi(0), \dots, \pi(t_0)\} \mid \mathcal{E}\right\} &> 1 - (k - (t_0 + 1)) \exp\left(-\frac{1}{25}k^{1-\delta}\right) \\ &> 1 - k \exp\left(-\frac{1}{25}k^{1-\delta}\right). \end{aligned} \quad (75)$$

We recall that $\mathbf{B}_{\text{alt},i}$ is the fraction of left nodes recovered when degree-1 right nodes run out in the alternative graph process on subgraph $i \in [r]$. Then, using (66) and (75), for all $N_{Di} \geq 1$ and $\mathbf{A}_i \geq \alpha_i^*$, we have for sufficiently large k :

$$\begin{aligned} \mathbb{P}\{\mathbf{B}_{\text{alt},i} = 1 \mid N_{Di}, \mathbf{A}_i\} &\geq \mathbb{P}\{\mathcal{E}\} \mathbb{P}\left\{S_l^{(t_0+1)} \geq 1, \forall l \in [k] \setminus \{\pi(0), \dots, \pi(t_0)\} \mid \mathcal{E}\right\} \\ &> \left[1 - \exp\left(-\frac{1}{20}k^{1-\delta}\right)\right] \left[1 - k \exp\left(-\frac{1}{25}k^{1-\delta}\right)\right] \\ &> 1 - \exp\left(-\frac{1}{30}k^{1-\delta}\right). \end{aligned} \quad (76)$$

This proves (55), and the result of Lemma 3.2 follows via (54). \square

5.4 Proof of Lemma 3.3

At the start of stage A, the pruned bipartite graph for a non-symmetric matrix \mathbf{X} as defined in Lemma 3.3 has $r\beta k^2$ left nodes and $R = dr\beta k^2/(\delta \ln k)$ right nodes. The proof of (17) is along the same lines as that of (14). Specifically, we first obtain a concentration inequality similar to (44) on the number of singleton right nodes in the initial graph. The subsequent steps are very similar to (48)–(49) and (52)–(53) and are omitted for brevity.

5.5 Proof of Lemma 3.4

Recall that the vectors in each of the sets $\{\mathbf{u}_1, \dots, \mathbf{u}_r\}$ and $\{\mathbf{v}_1, \dots, \mathbf{v}_r\}$ have k and βk disjoint supports, respectively, for some constant $\beta \in (0, 1]$. Thus, the nonzero entries of $\mathbf{X} = \sum_{i=1}^r \sigma_i \mathbf{u}_i \mathbf{v}_i^T = \sum_{i=1}^r \tilde{\mathbf{u}}_i \tilde{\mathbf{v}}_i^T$ form r disjoint submatrices, each of size $k \times \beta k$. The initial graph for stage B consists of r disjoint bipartite subgraphs. The peeling algorithm in stage B is applied to each of these subgraphs. In the i -th subgraph, the $(k + \beta k)$ left nodes represent the unknown nonzeros in $\tilde{\mathbf{u}}_i$ and $\tilde{\mathbf{v}}_i$. The $A_i \beta k^2$ right nodes represent the nonzero pairwise products recovered in the i -th nonzero submatrix in stage A.

As in the proof of the symmetric case, we will consider an alternative initial graph in which for each subgraph i , the $A_i \beta k^2$ right nodes are drawn uniformly at random *with replacement* from the set of βk^2 nonzero pairwise products in the i -th nonzero submatrix. See Fig. 14a for an illustration. The number of distinct right nodes for the alternative initial graph can be no larger than that for the original one. Moreover, as illustrated in Fig. 14, following the recovery of the first nonzero entry of $\tilde{\mathbf{u}}_i$, the process on the alternative graph peels off all the recoverable entries of $\tilde{\mathbf{v}}_i$ before peeling any nonzero entries of $\tilde{\mathbf{u}}_i$ that have become recoverable along the way. The order of peeling does not affect the total number of nonzeros recoverable in $\tilde{\mathbf{u}}_i$ and $\tilde{\mathbf{v}}_i$ before degree-1 right nodes run out.

Writing $B_{\text{alt},i}^u$ and $B_{\text{alt},i}^v$ for the fractions of nonzeros recoverable in $\tilde{\mathbf{u}}_i$ and $\tilde{\mathbf{v}}_i$ in the alternative process, we therefore have

$$\mathbb{P} \left\{ \{B_{\text{alt},i}^u < 1\} \cup \{B_{\text{alt},i}^v < 1\} \mid A_i \right\} \geq \mathbb{P} \left\{ \{B_i^u < 1\} \cup \{B_i^v < 1\} \mid A_i \right\}. \quad (77)$$

To prove (18), we will show that for $A_i \geq \alpha_i^*$ and sufficiently large k :

$$\mathbb{P} \left\{ \{B_{\text{alt},i}^u < 1\} \cup \{B_{\text{alt},i}^v < 1\} \mid A_i \right\} \leq \exp \left(-\frac{\beta}{8} k^{1-2\delta} \right), \quad i \in [r]. \quad (78)$$

The following lemma specifies the degree distribution of each left node at the beginning of stage B. The proof is along the same lines as that of Lemma 5.6 and is omitted.

Lemma 5.9 (Initial left degrees are Binomial). *Let Z_l^u be the degree of the left node representing the l -th nonzero of $\tilde{\mathbf{u}}_i$, and Z_j^v be the degree of the left node representing the j -th nonzero of $\tilde{\mathbf{v}}_i$, for $l \in [k]$ and $j \in [\beta k]$. Then,*

$$Z_l^u \sim \text{Bin} \left(A_i \beta k^2, \frac{1}{k} \right), \quad Z_j^v \sim \text{Bin} \left(A_i \beta k^2, \frac{1}{\beta k} \right). \quad (79)$$

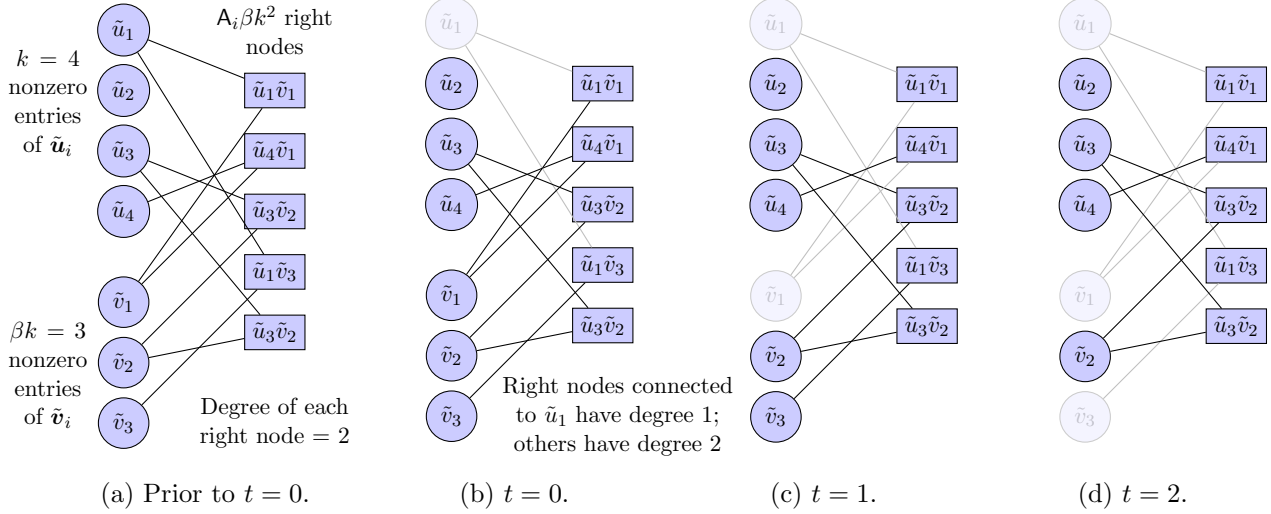


Figure 14: Alternative graph process showing the recovery of $\tilde{\mathbf{u}}_i$ and $\tilde{\mathbf{v}}_i$ given \mathbf{A}_i (as the counterpart of Fig. 3). The double occurrence of $\tilde{u}_3\tilde{v}_2$ as right nodes highlights that the right nodes are sampled *with replacement* from the βk^2 nonzero pairwise products in the nonzero submatrix corresponding to $\tilde{\mathbf{u}}_i\tilde{\mathbf{v}}_i^T$. (b): At $t = 0$, \tilde{u}_1 is recovered as 1 and peeled off. (c)–(d): Following the recovery of \tilde{u}_1 , we peel off all the recoverable \tilde{v}_j 's (i.e., \tilde{v}_1, \tilde{v}_3) before peeling any \tilde{u}_l 's that have become recoverable along the way (i.e., \tilde{u}_4).

Then, for $\mathbf{A}_i \geq \alpha_i^*$ and sufficiently large k :

$$\mathbb{P} \left\{ Z_l^u \notin \left[\frac{\mathbf{A}_i \beta k}{2}, \frac{3\mathbf{A}_i \beta k}{2} \right] \mid \mathbf{A}_i \right\} < 2 \exp \left(-\frac{\beta}{10} k^{1-\delta} \right), \quad (80)$$

$$\mathbb{P} \left\{ Z_j^v \notin \left[\frac{\mathbf{A}_i k}{2}, \frac{3\mathbf{A}_i k}{2} \right] \mid \mathbf{A}_i \right\} < 2 \exp \left(-\frac{1}{10} k^{1-\delta} \right). \quad (81)$$

Define the event

$$\mathcal{T}_0 := \left\{ Z_l^u \in \left[\frac{\mathbf{A}_i \beta k}{2}, \frac{3\mathbf{A}_i \beta k}{2} \right], \forall l \in [k] \right\} \cap \left\{ Z_j^v \in \left[\frac{\mathbf{A}_i k}{2}, \frac{3\mathbf{A}_i k}{2} \right], \forall j \in [\beta k] \right\}. \quad (82)$$

Then for $\mathbf{A}_i \geq \alpha_i^*$ and sufficiently large k :

$$\mathbb{P} \{ \mathcal{T}_0 \mid \mathbf{A}_i \} > 1 - 2k \exp \left(-\frac{\beta}{10} k^{1-\delta} \right) - 2\beta k \exp \left(-\frac{1}{10} k^{1-\delta} \right). \quad (83)$$

The recovery of each nonzero entry of $\tilde{\mathbf{u}}_i$ or $\tilde{\mathbf{v}}_i$ is counted as one iteration of the algorithm. The recovery of the first nonzero entry of $\tilde{\mathbf{u}}_i$ or $\tilde{\mathbf{v}}_i$ corresponds to iteration $t = 0$. The next lemma specifies the distribution of degree-1 right nodes connected to each remaining left node after each iteration of the algorithm. The proof is similar to that of Lemma 5.7 and is omitted for brevity.

Lemma 5.10 (Number of degree-1 right nodes connected to each unpeeled left node). *Suppose that the peeling algorithm on the i -th subgraph has not terminated after iteration $(t - 1)$, for $1 \leq t \leq (k + \beta k - 1)$. Let $\mathcal{U}(t - 1)$ and $\mathcal{V}(t - 1)$ be the set of indices of the nonzeros recovered in $\tilde{\mathbf{u}}_i$ and $\tilde{\mathbf{v}}_i$ by the end of iteration $(t - 1)$. At the start of iteration t , let $S_1^{(u,t)}$ be the number of degree-1*

right nodes connected to the remaining left node \tilde{u}_l and let $S_j^{(v,t)}$ be that connected to the remaining left node \tilde{v}_j , where $l \in [k] \setminus \mathcal{U}(t-1)$ and $j \in [\beta k] \setminus \mathcal{V}(t-1)$. Then,

$$S_l^{(u,t)} \sim \text{Bin}\left(\mathbf{A}_i \beta k^2, \frac{|\mathcal{V}(t-1)|}{\beta k^2}\right), \quad S_j^{(v,t)} \sim \text{Bin}\left(\mathbf{A}_i \beta k^2, \frac{|\mathcal{U}(t-1)|}{\beta k^2}\right). \quad (84)$$

In the following, we refer to the left nodes representing the nonzero entries of $\tilde{\mathbf{u}}_i$ as \tilde{u} -left nodes, and those representing nonzero entries of $\tilde{\mathbf{v}}_i$ as \tilde{v} -left nodes. We assume without loss of generality that the peeling algorithm is initialized by setting a \tilde{u} -left node to 1. As illustrated in Fig. 14b, following the recovery of the first \tilde{u} -left node, all the right nodes connected to this node reduce to degree-1. The next lemma gives a high probability lower bound on the number of degree-1 right nodes created.

Lemma 5.11 (Recovery of the first left node). *Denote by N the number of distinct \tilde{v} -left nodes connected to the degree-1 right nodes created by the recovery of the first \tilde{u} -left node. Then, there exists $b_{k,\delta} = o(k^{1-\delta})$ such that for $\mathbf{A}_i \geq \alpha_i^*$ and sufficiently large k , we have*

$$\mathbb{P}\left\{N \geq \frac{\beta}{2}k^{1-\delta} - b_{k,\delta} \mid \mathcal{T}_0, \mathbf{A}_i\right\} \geq 1 - 2 \exp\left(-\frac{\beta}{2}k^{1-\frac{3}{2}\delta}\right). \quad (85)$$

Here \mathcal{T}_0 is the event defined in (82).

Proof. Let Z^u be the degree of the first \tilde{u} -left node recovered. Then the recovery of this \tilde{u} -left node creates Z^u degree-1 right nodes. Consider a \tilde{v} -left node, say \tilde{v}_j , and let S_j^v be the number of degree-1 right nodes connected to \tilde{v}_j after the first \tilde{u} -left node is peeled off. Then, conditioned on Z^u , we have

$$S_j^v := \sum_{s=1}^{Z^u} \mathbb{1}\{\text{The } s\text{-th degree-1 right node is connected to } \tilde{v}_j\} \sim \text{Bin}\left(Z^u, \frac{1}{\beta k}\right), \quad \text{for } j \in [\beta k], \quad (86)$$

and we can express N (defined in the lemma statement) as

$$N := \sum_{j=1}^{\beta k} \mathbb{1}\{S_j^v \geq 1\}. \quad (87)$$

Let V_s be the index of the \tilde{v} -left node that the s -th degree-1 right node is connected to, for $s \in [Z^u]$. Let $N_0 = \mathbb{E}[N \mid Z^u, \mathbf{A}_i]$ and

$$N_s = \mathbb{E}[N \mid V_1, \dots, V_s, Z^u, \mathbf{A}_i], \quad s \in [Z^u]. \quad (88)$$

Conditioned on Z^u , the sequence $\{N_s\}$ is a Doob Martingale, with $N_{Z^u} = N$. Writing $N = f(V_1, \dots, V_{Z^u})$, we note that f is 1-Lipschitz since changing the connection of a single right node cannot change N by more than one. Moreover, by the construction of the alternative graph, V_1, \dots, V_{Z^u} are independent given (Z^u, \mathbf{A}_i) . Therefore, by McDiarmid's inequality [50, Sec. 13.5], we have

$$\mathbb{P}\left\{|N - \mathbb{E}[N \mid Z^u, \mathbf{A}_i]| \geq k^{-\frac{\delta}{4}} Z^u \mid Z^u, \mathbf{A}_i\right\} \leq 2 \exp\left(-2k^{-\frac{\delta}{2}} Z^u\right). \quad (89)$$

Hence

$$\mathbb{P}\left\{N \geq \mathbb{E}[N \mid Z^u, \mathbf{A}_i] - k^{-\frac{\delta}{4}} Z^u \mid Z^u, \mathbf{A}_i\right\} \geq 1 - 2 \exp\left(-2k^{-\frac{\delta}{2}} Z^u\right). \quad (90)$$

From (86) and (87), we obtain that

$$\mathbb{E}[N \mid Z^u, \mathbf{A}_i] = \beta k \mathbb{P}\{S_j^v \geq 1\} = \beta k \left[1 - \left(1 - \frac{1}{\beta k}\right)^{Z^u} \right] \geq \beta k \left(1 - \exp\left(-\frac{Z^u}{\beta k}\right)\right). \quad (91)$$

Furthermore, given $\mathbf{A}_i \geq \alpha_i^* = k^{-\delta} - o(k^{-\delta})$ and conditioning on \mathcal{T}_0 , we have

$$Z^u \geq \frac{\beta}{2} k^{1-\delta} - o(k^{1-\delta}), \quad \mathbb{E}[N \mid Z^u, \mathbf{A}_i] - k^{-\frac{\delta}{4}} Z^u \geq \frac{\beta}{2} k^{1-\delta} - o(k^{1-\delta}). \quad (92)$$

Using (92) in (90) gives the result in (85). \square

Proof of Lemma 3.4. With N as defined in Lemma 5.11, at the end of iteration N of the peeling algorithm, one \tilde{u} -left node and N \tilde{v} -left nodes have been recovered. Adopting the notation in Lemma 5.10, this means $|\mathcal{U}(N)| = 1$ and $|\mathcal{V}(N)| = N$. Lemma 5.10 implies that at the start of iteration $(N+1)$, the number of degree-1 right nodes connected to each remaining \tilde{u} -left node is

$$S_l^{(u, N+1)} \sim \text{Bin}\left(\mathbf{A}_i \beta k^2, \frac{N}{\beta k^2}\right), \quad \text{for } l \in [k] \setminus \mathcal{U}(N). \quad (93)$$

Recall the definition of \mathcal{T}_0 from (82) and let

$$\mathcal{T}_1 := \left\{ N \geq \frac{\beta}{2} k^{1-\delta} - b_{k,\delta} \right\}, \quad \mathcal{T}_2 := \left\{ S_l^{(u, N+1)} \geq 1, \forall l \in [k] \setminus \mathcal{U}(N) \right\}. \quad (94)$$

Here $b_{k,\delta} = o(k^{1-\delta})$ is the same as in Lemma 5.11. Note that \mathcal{T}_2 is the event that at the start of iteration $(N+1)$, each of the $(k-1)$ remaining \tilde{u} -left nodes is connected to at least one degree-1 right node and can therefore be recovered. Analogously to (74) and (75), we can show that for $\mathbf{A}_i \geq \alpha_i^*$ and sufficiently large k ,

$$\mathbb{P}\{\mathcal{T}_2 \mid \mathcal{T}_0, \mathcal{T}_1, \mathbf{A}_i\} > 1 - (k-1) \exp\left(-\frac{\beta}{4} k^{1-2\delta}\right). \quad (95)$$

Since the recovery of each left node corresponds to one iteration, conditioned on the event \mathcal{T}_2 , we have $|\mathcal{U}(N+k-1)| = k$ and $|\mathcal{V}(N+k-1)| = N$.

At the start of iteration $(N+k)$, all the left nodes that remain are \tilde{v} -left nodes, so all the right nodes that remain are degree-1. Moreover, for $\mathbf{A}_i \geq \alpha_i^*$ and sufficiently large k , conditioning on event \mathcal{T}_0 ensures that each \tilde{v} -left node is connected to at least one right node. Therefore, all the remaining \tilde{v} -left nodes can be recovered. If the events $\mathcal{T}_0, \mathcal{T}_1, \mathcal{T}_2$ all hold, then the algorithm successfully recovers all the nonzeros of $\tilde{\mathbf{u}}_i$ and $\tilde{\mathbf{v}}_i$. Indeed, we have for $\mathbf{A}_i \geq \alpha_i^*$ and sufficiently large k :

$$\begin{aligned} & \mathbb{P}\left\{ \{\mathbf{B}_{\text{alt},i}^u = 1\} \cap \{\mathbf{B}_{\text{alt},i}^v = 1\} \mid \mathbf{A}_i \right\} \\ & \geq \mathbb{P}\{\mathcal{T}_0, \mathcal{T}_1, \mathcal{T}_2 \mid \mathbf{A}_i\} \\ & = \mathbb{P}\{\mathcal{T}_0 \mid \mathbf{A}_i\} \mathbb{P}\{\mathcal{T}_1 \mid \mathcal{T}_0, \mathbf{A}_i\} \mathbb{P}\{\mathcal{T}_2 \mid \mathcal{T}_0, \mathcal{T}_1, \mathbf{A}_i\} \\ & \stackrel{(i)}{>} \left[1 - 2k \exp\left(-\frac{\beta}{10} k^{1-\delta}\right) - 2\beta k \exp\left(-\frac{1}{10} k^{1-\delta}\right) \right] \left[1 - 2 \exp\left(-\frac{\beta}{2} k^{1-\frac{3}{2}\delta}\right) \right] \\ & \quad \cdot \left[1 - (k-1) \exp\left(-\frac{\beta}{4} k^{1-2\delta}\right) \right] \\ & > 1 - \exp\left(-\frac{\beta}{8} k^{1-2\delta}\right), \end{aligned} \quad (96)$$

where the inequality (i) is obtained using the bounds in (83), (85) and (95). This proves (78), and via (77), completes the proof of Lemma 3.4. □

6 Conclusion

The main contribution of this paper is a sketching scheme for sparse, low-rank matrices and an algorithm for recovering the singular vectors of such a matrix with a sample complexity and running time that both depend only on the sparsity level k and not on the ambient dimension n of the matrix.

A key open question in the noiseless setting is how to extend the two-stage recovery algorithm to matrices where the singular vectors have overlapping supports. A starting point in this direction would be to consider matrices whose singular vectors have a small fraction of nonzero entries in overlapping locations. This would ensure that a large fraction of the nonzero matrix entries recovered in stage A are still simple pairwise products. Moreover, we would like to improve the guarantees in part 2) of Theorems 1 and 2, via a proof similar to that of part 1), using properties of negatively associated random variables. This would also give tighter non-asymptotic bounds for the compressed sensing scheme in [1].

There are several open questions in the noisy setting where the matrix is only approximately sparse and low-rank. An important one is to improve the running time of the recovery algorithm, which is currently $\mathcal{O}(\max\{n^2 \log(n/k), (rk)^3\})$. This will require the sketching operator to be defined via a new bin detection matrix \mathbf{S} which enables zero-ton and singleton bins to be identified more efficiently. In our construction, for simplicity, we chose \mathbf{S} to be a random Gaussian matrix. For compressed sensing, [1] proposed an \mathbf{S} based on LDPC codes that allows for faster classification of the bins via a message passing algorithm. It would be interesting to explore similar ideas for matrix sketching. Another future direction is to derive performance guarantees for the noisy setting, similar to the nonasymptotic bounds derived in the noiseless case. It is possible to obtain guarantees for the first stage of the algorithm, similarly to [1], but the challenge lies in quantifying how the noisy recovery in the first stage affects the recovery accuracy in the second stage.

Acknowledgements

The authors thank Prof. Kannan Ramchandran, Dr. Dong Yin and Dr. Orhan Ocal for several helpful discussions about the compressed sensing scheme in [1], Dr. Samet Oymak for discussions regarding [32], and Prof. Justin Romberg and Dr. Sohail Bahmani for sharing their source code for [33] and discussions regarding implementation details. The authors also thank Dr. Mark L. Stone and Dr. Stephen Becker for answering questions about CVX and TFOCS.

References

- [1] X. Li, D. Yin, S. Pawar, R. Pedarsani, and K. Ramchandran, “Sub-linear time support recovery for compressed sensing using sparse-graph codes,” *IEEE Transactions on Information Theory*, vol. 65, no. 10, pp. 6580–6619, 2019.
- [2] M. Bakshi, S. Jaggi, S. Cai, and M. Chen, “Sho-fa: Robust compressive sensing with order-optimal complexity, measurements, and bits,” *IEEE Transactions on Information Theory*, vol. 62, no. 12, pp. 7419–7444, 2016.

- [3] D. P. Woodruff, “Sketching as a tool for numerical linear algebra,” *Foundations and Trends in Theoretical Computer Science*, vol. 10, no. 1-2, pp. 1–157, 2014.
- [4] J. A. Tropp, A. Yurtsever, M. Udell, and V. Cevher, “Practical sketching algorithms for low-rank matrix approximation,” *SIAM Journal on Matrix Analysis and Applications*, vol. 38, no. 4, pp. 1454–1485, 2017.
- [5] X. Ma, L. Xiao, and W. H. Wong, “Learning regulatory programs by threshold svd regression,” *Proceedings of the National Academy of Sciences*, vol. 111, no. 44, pp. 15 675–15 680, 2014.
- [6] Z. Ma, Z. Ma, and T. Sun, “Adaptive estimation in two-way sparse reduced-rank regression,” *Statistica Sinica*, vol. 30, no. 4, pp. 2179–2201, 2020.
- [7] H. Zou, T. Hastie, and R. Tibshirani, “Sparse principal component analysis,” *Journal of Computational and Graphical Statistics*, vol. 15, no. 2, pp. 265–286, 2006.
- [8] T. Hastie, R. Tibshirani, and M. Wainwright, *Statistical Learning with Sparsity: the Lasso and Generalizations*. Chapman and Hall/CRC, 2015.
- [9] K. Lee, Y. Wu, and Y. Bresler, “Near-optimal compressed sensing of a class of sparse low-rank matrices via sparse power factorization,” *IEEE Transactions on Information Theory*, vol. 64, no. 3, pp. 1666–1698, 2018.
- [10] M. Girvan and M. E. J. Newman, “Community structure in social and biological networks,” *Proceedings of the National Academy of Sciences*, vol. 99, no. 12, pp. 7821–7826, 2002.
- [11] Daxin Jiang, Chun Tang, and Aidong Zhang, “Cluster analysis for gene expression data: a survey,” *IEEE Transactions on Knowledge and Data Engineering*, vol. 16, no. 11, pp. 1370–1386, 2004.
- [12] M. Lee, H. Shen, J. Z. Huang, and J. S. Marron, “Biclustering via sparse singular value decomposition,” *Biometrics*, vol. 66, no. 4, pp. 1087–1095, 2010.
- [13] E. Richard, P.-A. Savalle, and N. Vayatis, “Estimation of simultaneously sparse and low rank matrices,” in *Proceedings of the 29th International Conference on Machine Learning (ICML)*, 2012.
- [14] S. Pawar and K. Ramchandran, “Ffast: An algorithm for computing an exactly k -sparse DFT in $o(k \log k)$ time,” *IEEE Transactions on Information Theory*, vol. 64, no. 1, pp. 429–450, 2018.
- [15] N. T. Janakiraman, S. Emmadi, K. Narayanan, and K. Ramchandran, “Exploring connections between sparse Fourier transform computation and decoding of product codes,” in *Proc. 53rd Annual Allerton Conference on Communication, Control, and Computing*, 2015, pp. 1366–1373.
- [16] X. Li, J. K. Bradley, S. Pawar, and K. Ramchandran, “SPRIGHT: A fast and robust framework for sparse Walsh-Hadamard transform,” arXiv:1508.06336, 2015.
- [17] R. Scheibler, S. Haghghatshoar, and M. Vetterli, “A fast Hadamard transform for signals with sublinear sparsity in the transform domain,” *IEEE Transactions on Information Theory*, vol. 61, no. 4, pp. 2115–2132, 2015.
- [18] X. Chen and D. Guo, “Robust sublinear complexity Walsh-Hadamard transform with arbitrary sparse support,” in *Proc. IEEE International Symposium on Information Theory*, 2015, pp. 2573–2577.
- [19] S. Cai, M. Bakshi, S. Jaggi, and M. Chen, “Super: Sparse signals with unknown phases efficiently recovered,” in *Proc. IEEE International Symposium on Information Theory*, 2014, pp. 2007–2011.
- [20] R. Pedarsani, D. Yin, K. Lee, and K. Ramchandran, “Phasecode: Fast and efficient compressive phase retrieval based on sparse-graph codes,” *IEEE Transactions on Information Theory*, vol. 63, no. 6, pp. 3663–3691, 2017.
- [21] R. Pedarsani, K. Lee, and K. Ramchandran, “Sparse covariance estimation based on sparse-graph codes,” in *53rd Annual Allerton Conference on Communication, Control, and Computing*, 2015, pp. 612–619.

- [22] X. Li and K. Ramchandran, “An active learning framework using sparse-graph codes for sparse polynomials and graph sketching,” in *Advances in Neural Information Processing Systems*, vol. 28, 2015.
- [23] D. Yin, R. Pedarsani, Y. Chen, and K. Ramchandran, “Learning mixtures of sparse linear regressions using sparse graph codes,” *IEEE Transactions on Information Theory*, vol. 65, no. 3, pp. 1430–1451, 2019.
- [24] M. G. Luby, M. Mitzenmacher, M. A. Shokrollahi, and D. A. Spielman, “Efficient erasure correcting codes,” *IEEE Transactions on Information Theory*, vol. 47, no. 2, pp. 569–584, 2001.
- [25] T. Richardson and R. Urbanke, *Modern Coding Theory*. New York: Cambridge University Press, 2008.
- [26] D. Dubhashi and D. Ranjan, “Balls and bins: A study in negative dependence,” *Random Structures & Algorithms*, vol. 13, no. 2, pp. 99–124, 1998.
- [27] M. A. Davenport and J. Romberg, “An overview of low-rank matrix recovery from incomplete observations,” *IEEE Journal of Selected Topics in Signal Processing*, vol. 10, no. 4, pp. 608–622, Jun 2016.
- [28] B. Recht, M. Fazel, and P. A. Parrilo, “Guaranteed minimum-rank solutions of linear matrix equations via nuclear norm minimization,” *SIAM review*, vol. 52, no. 3, pp. 471–501, 2010.
- [29] E. J. Candès and Y. Plan, “Tight oracle inequalities for low-rank matrix recovery from a minimal number of noisy random measurements,” *IEEE Transactions on Information Theory*, vol. 57, no. 4, pp. 2342–2359, 2011.
- [30] T. Wimalajeewa, Y. C. Eldar, and P. K. Varshney, “Recovery of sparse matrices via matrix sketching,” arXiv:1311.2448, 2013.
- [31] G. Dasarathy, P. Shah, B. N. Bhaskar, and R. D. Nowak, “Sketching sparse matrices, covariances, and graphs via tensor products,” *IEEE Transactions on Information Theory*, vol. 61, no. 3, pp. 1373–1388, 2015.
- [32] S. Oymak, A. Jalali, M. Fazel, Y. C. Eldar, and B. Hassibi, “Simultaneously structured models with application to sparse and low-rank matrices,” *IEEE Transactions on Information Theory*, vol. 61, no. 5, pp. 2886–2908, 2015.
- [33] S. Bahmani and J. Romberg, “Near-optimal estimation of simultaneously sparse and low-rank matrices from nested linear measurements,” *Information and Inference: A Journal of the IMA*, vol. 5, no. 3, pp. 331–351, 2016.
- [34] Y. Chen, Y. Chi, and A. J. Goldsmith, “Exact and stable covariance estimation from quadratic sampling via convex programming,” *IEEE Transactions on Information Theory*, vol. 61, no. 7, pp. 4034–4059, 2015.
- [35] S. Bahmani and J. Romberg, “Sketching for simultaneously sparse and low-rank covariance matrices,” in *IEEE 6th International Workshop on Computational Advances in Multi-Sensor Adaptive Processing*, 2015, pp. 357–360.
- [36] E. J. Candès, T. Strohmer, and V. Voroninski, “Phaselift: Exact and stable signal recovery from magnitude measurements via convex programming,” *Communications on Pure and Applied Mathematics*, vol. 66, no. 8, pp. 1241–1274, 2013.
- [37] I. M. Johnstone and A. Y. Lu, “On consistency and sparsity for principal components analysis in high dimensions,” *Journal of the American Statistical Association*, vol. 104, no. 486, pp. 682–693, 2009.
- [38] A. A. Amini and M. J. Wainwright, “High-dimensional analysis of semidefinite relaxations for sparse principal components,” *The Annals of Statistics*, vol. 37, no. 5B, pp. 2877 – 2921, 2009.
- [39] A. Birnbaum, I. M. Johnstone, B. Nadler, and D. Paul, “Minimax bounds for sparse PCA with noisy high-dimensional data,” *The Annals of Statistics*, vol. 41, no. 3, pp. 1055 – 1084, 2013.

- [40] A. Ahmed, B. Recht, and J. Romberg, “Blind deconvolution using convex programming,” *IEEE Transactions on Information Theory*, vol. 60, no. 3, pp. 1711–1732, 2014.
- [41] M. Grant and S. Boyd, “CVX: Matlab software for disciplined convex programming, version 2.1,” <http://cvxr.com/cvx>, Mar. 2014.
- [42] —, “Graph implementations for nonsmooth convex programs,” in *Recent Advances in Learning and Control*, ser. Lecture Notes in Control and Information Sciences, V. Blondel, S. Boyd, and H. Kimura, Eds. Springer-Verlag Limited, 2008, pp. 95–110.
- [43] *MOSEK Optimization Toolbox for MATLAB 10.0.25*, Oct. 2022. [Online]. Available: <https://docs.mosek.com/latest/toolbox/index.html>
- [44] S. Becker, E. Candes, and M. Grant, *TFOCS user guide Version 1.3 release 2*, Oct. 2014. [Online]. Available: <http://cvxr.com/tfocs/doc>
- [45] G. W. Anderson, A. Guionnet, and O. Zeitouni, *An Introduction to Random Matrices*, ser. Cambridge Studies in Advanced Mathematics. Cambridge University Press, 2009.
- [46] J. Yang and Y. Zhang, “Alternating direction algorithms for ℓ_1 -problems in compressive sensing,” *SIAM Journal on Scientific Computing*, vol. 33, no. 1, pp. 250–278, 2011.
- [47] Y. Zhang, W. Deng, J. Yang, and W. Yin, *YALL1: Your ALgorithms for L1*, Jul. 2011. [Online]. Available: <https://yall1.blogs.rice.edu>
- [48] T. M. Cover and J. A. Thomas, *Elements of Information Theory*. USA: Wiley-Interscience, 2006.
- [49] K. Joag-Dev and F. Proschan, “Negative Association of Random Variables with Applications,” *The Annals of Statistics*, vol. 11, no. 1, pp. 286 – 295, 1983.
- [50] M. Mitzenmacher and E. Upfal, *Probability and Computing: Randomization and Probabilistic Techniques in Algorithms and Data Analysis*, 2nd ed. USA: Cambridge University Press, 2017.